Doctoral Dissertation (Censored)

博士論文（要約）

# In-situ Radiation-mode Optical Microscopy and XPS Study of Chemical Vapor Deposition Growth of Graphene

（その場観測熱放射光学顕微法および X 線光電子分光法による
グラフェン化学気相成長の研究）

A Dissertation Submitted for the Degree of Doctor of Science

December 2020

令和 2 年 12 月 博士（理学）申請

Department of Chemistry, Graduate School of Science,
The University of Tokyo
東京大学大学院理学系研究科化学専攻

Takanobu Taira

平良 隆信

# Abstract

Graphene is a monolayer of graphite that has attracted widespread attention because of its outstanding properties. Scalable and rapid production of graphene is required for its industrial applications. Chemical vapor deposition (CVD) is considered the most promising method to synthesize large-area single-crystalline graphene. In a typical CVD process of graphene, $CH_4$ with Ar and $H_2$ is supplied onto a Cu foil substrate at a temperature of about 1000 °C, where $CH_4$ molecules are decomposed to form graphene nuclei. When the density of graphene nucleation is high, the resulting graphene becomes polycrystalline graphene, which exhibits inferior properties to those of single-crystalline graphene. To rapidly produce large-area single-crystalline graphene, suppressing graphene nucleation and accelerating growth must be simultaneously realized. For this purpose, the effects of various parameters such as gas flow rate, total pressure, and substrate temperature on CVD growth of graphene must be elucidated.

Herein, I systematically investigated the effects of two factors: (1) hot filament and (2) hydrogen. In hot-filament-assisted CVD (HF-CVD), the source gas is decomposed by a high-temperature filament before it reaches the substrate. Therefore, the hot filament is a potential candidate for growth acceleration. However, its effects on nucleation and growth are unclear. $H_2$ is generally supplied with $CH_4$ onto a Cu foil substrate. Varying effects of hydrogen on the nucleation, growth, and etching of graphene have been reported, but some of the effects seemed inconsistent with others and the major effect remains unclear. One of the reasons for the uncertainty is that the effects were evaluated by ex-situ observation after finishing the graphene growth, which cannot accurately evaluate the nucleation and growth rate. To elucidate the aforementioned effects, in-situ observation of the CVD growth of graphene would be required.

In this study, I used radiation-mode optical microscopy (Rad-OM), which can visualize graphene growth in real time by utilizing the difference in emissivity of graphene and Cu. Further, I combined the Rad-OM with in-situ synchrotron radiation X-ray photoelectron spectroscopy (SR-XPS) to characterize the surface species and evaluate the effect of hydrogen.

I investigated the effect of the hot filament using Rad-OM. I proved that the use of the hot filament induced additional nucleation and enhanced the growth rate; further, the hot filament at optimized temperatures is expected to accelerate growth without causing additional nucleation. Therefore, the hot filament would be useful for the rapid synthesis of large-area single-crystalline graphene.

I investigated the effect of hydrogen using Rad-OM and the combined Rad-OM and in-situ SR-XPS measurements. Both Rad-OM and SR-XPS results revealed that hydrogen etched graphene during the growth and annealing processes. Based on these findings, I concluded that the main effect of hydrogen on graphene is etching. The etching effect of hydrogen suppresses the nucleation of graphene domains during growth. Thus, introducing $H_2$ is beneficial for the growth of large-area single-crystalline graphene domains.

These conclusions based on the in-situ Rad-OM and SR-XPS measurements will be useful for establishing guidelines to optimize the CVD growth of graphene and will pave the way for the production of large-area single-crystalline graphene.

# Contents

# Chapter 1. Introduction

In this chapter, the structure, properties, and applications of graphene are described. Then, the overview, challenges, and methods for the evaluation of the chemical vapor deposition (CVD) growth of graphene, which is the most promising method of graphene synthesis for industrial applications, are detailed. Finally, the purpose of the study is outlined.

## 1.1. Graphene

Graphene is a monolayer of graphite, consisting of an $sp^2$ carbon lattice. It was first exfoliated from graphite by Novoselov *et al*. in 2004 [1]. Subsequently, it garnered significant attention because of its outstanding properties, such as high carrier mobility [2], excellent mechanical strength [3], and high transparency [4].

The discovery of graphene has opened up the science of other atomic layer materials, such as monolayers of hexagonal boron nitride (h-BN) [5], molybdenum disulfide ($MoS_2$) [6], silicene (Si) [7], and germanene (Ge) [8]. In particular, the properties and stacking of various materials [9], [10] have been eagerly investigated.

The use of graphene for applications in high-speed electronic devices [11], sensors for detecting gases [12] or viruses [13], touch panels [14], and so on [15] has been reported, but graphene has limited industrial use. This is because its manufacturing methods are still developing. The production of graphene for industrial applications necessitates the effective synthesis of high-quality wafer-scale (~ 4 in.) graphene. The quality of graphene is mainly evaluated based on its carrier mobility [16], [17], and the quality is affected by crystallinity, defects, and the layer number of graphene. The mobility of single-crystalline graphene is higher than that of polycrystalline graphene because the domain boundary in polycrystalline graphene decreases the mobility and mechanical strength [18], [19]. Defects in the graphene lattice also degrade the properties. In addition, the mobility of monolayer graphene is higher than that of multilayer graphene [20]. Thus, wafer-scale single-crystalline monolayer graphene with few defects needs to be effectively synthesized.

The representative proposed methods for fabricating graphene are mechanical exfoliation [1], chemical exfoliation [21], SiC decomposition [22], and chemical vapor deposition (CVD) [23]. To date, mechanical exfoliation produces the highest quality graphene by repeatedly peeling off bulk graphite (highly oriented pyrolytic graphite, HOPG) with a cellophane adhesive tape to isolate a monolayer of graphene. However, mechanical exfoliation exhibits the lowest productivity because the peeling process is time-consuming and the acquired graphene has dimensions of only a few micrometers. Chemical exfoliation, which exfoliates graphite by oxidation with acid, provides the highest productivity because oxidation process is rapid. However, the obtained graphene is of poor quality because the process induces defects in the graphene. Both the quality of CVD-grown graphene and the productivity of CVD is the second highest [24]. Thus, further improvement of the quality and productivity of the CVD growth of graphene will enable it to become the most effective method for synthesizing high-quality graphene.

## 1.2. Chemical vapor deposition (CVD) growth of graphene

In the CVD growth of graphene, the carbon source gas (e.g., $CH_4$) is supplied onto a heated metal substrate (e.g., Cu). In this process, the gas molecule is adsorbed on the substrate and decomposed into carbon precursors by the catalytic activity of the metal substrate. Subsequently, the precursors diffuse on the substrate and aggregate to induce nucleation and growth of graphene [25]. When the density of the graphene nucleation is high, the resulting graphene becomes polycrystalline graphene, which exhibits inferior properties to single-crystalline graphene [18], [19] as shown in Figure 1.1. Thus, suppressing nucleation density of graphene is the key challenge for the synthesis of large-area single-crystalline graphene.

In 2009, Li *et al*. reported the first synthesis of micrometer-sized graphene by CVD in which $CH_4$, Ar, and $H_2$ were supplied onto a Cu foil substrate at 1000 °C [23]. They also demonstrated that the synthesized graphene could be transferred onto the $SiO_2$ substrate by coating Cu with polymethyl methacrylate (PMMA) and etching away the Cu [23], which is necessary for the applications of graphene. Thereafter, many experimental

and theoretical studies have investigated the effects of various parameters to further improve the size, quality, and growth rate of the CVD growth of graphene.

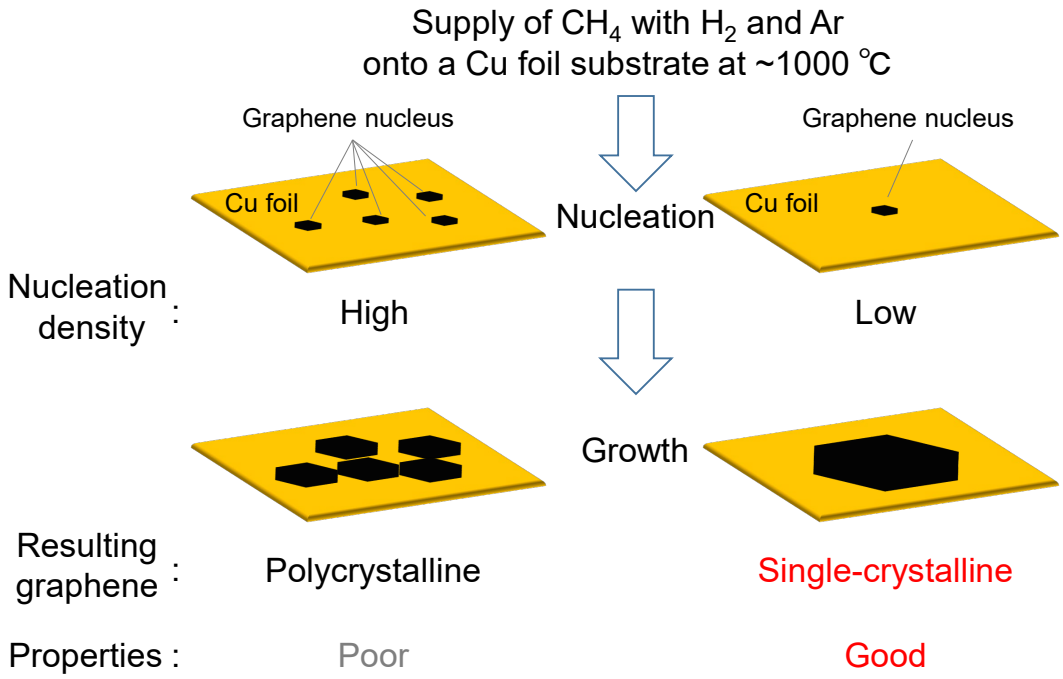


Figure 1.1 Schematic illustration of the CVD growth of graphene.

# 1.3. Growth parameters for CVD growth of graphene

The parameters impacting the CVD growth of graphene can be roughly categorized into two groups: (1) substrate parameters and (2) gas parameters.

## 1.3.1. Substrate parameters

The types of elements, impurities, morphology, pretreatment, and substrate temperature, were the substrate parameters investigated.

Various types of metals such as Cu, Ni, Co, Pt, Au, Ag, Fe, and Ir have been investigated as CVD substrates [17], [25]. Previous studies confirmed that Cu was the best substrate for the industrial production of monolayer graphene because $CH_4$ decomposition and graphene formation could occur on the Cu surface without the dissolution of carbon into the Cu bulk, owing to the low carbon solubility of Cu [26]. Conversely, carbon precursors dissolved into the bulk during CVD on high carbon solubility metals such as Ni, and precipitated onto the surface to form multilayer graphene during cooling to room temperature [26]. In industrial applications, inexpensive Cu foils are the preferred alternatives to expensive Cu single crystals because the Cu foil is etched during the transfer process after CVD growth [23], [27], [28]. Transfer-free methods for CVD growth of graphene, in which the source gas was directly supplied onto insulating substrates such as $SiO_2$ or h-BN [29]–[31], were also reported, but the quality and size of the synthesized graphene were inferior to those of graphene grown on Cu foil. Thus, graphene growth on Cu foil followed by transfer of CVD graphene onto an insulating substrate is the preferred method.

Cu foil generally has a larger amount of impurities, rougher morphology, and more grain boundaries (GBs) than Cu single crystal. Therefore, the effects of these parameters and the pretreatment methods for their optimization were investigated. Recent studies reported that carbon impurities on the Cu foil substrate are the dominant factor for graphene nucleation; therefore, the removal of carbon impurities is an effective pretreatment method for suppressing the number of nucleation sites. Kraus *et al*. and Braeuninger-Weimer *et al*. demonstrated that the amount of carbon impurities in a Cu substrate is proportional to the graphene nucleation density, and oxygen annealing can

effectively remove the carbon impurities, thereby suppressing nucleation [32], [33]. I reported that the carbon impurities functioned as nucleation sites (Figure 1.2) and were effectively removed by Ar bombardment (Figures 1.2–1.4), which was revealed by real-time observation using radiation-mode optical microscopy (Rad-OM) [34], which is described in Section 1.4. It was reported that the morphology or roughness of the substrate was not related to the graphene nucleation. The methods for flattening the Cu substrate by polishing or etching decreased the nucleation density [35]–[37], but simultaneously removed carbon impurities [32], [33]. I reported that the GBs in the Cu foil had little effect on the nucleation and lateral growth of the graphene domains (Figures 1.5 and 1.6) [38]. Therefore, it is the removal of the carbon impurities from the Cu foil substrate that is important for decreasing the nucleation density, rather than the modifying of the Cu morphology.

Larger graphene domains with fewer defects were grown at higher substrate temperatures. On the other hand, smaller graphene domains with more defects grew at lower temperatures because of insufficient decomposition of $CH_4$ [39].

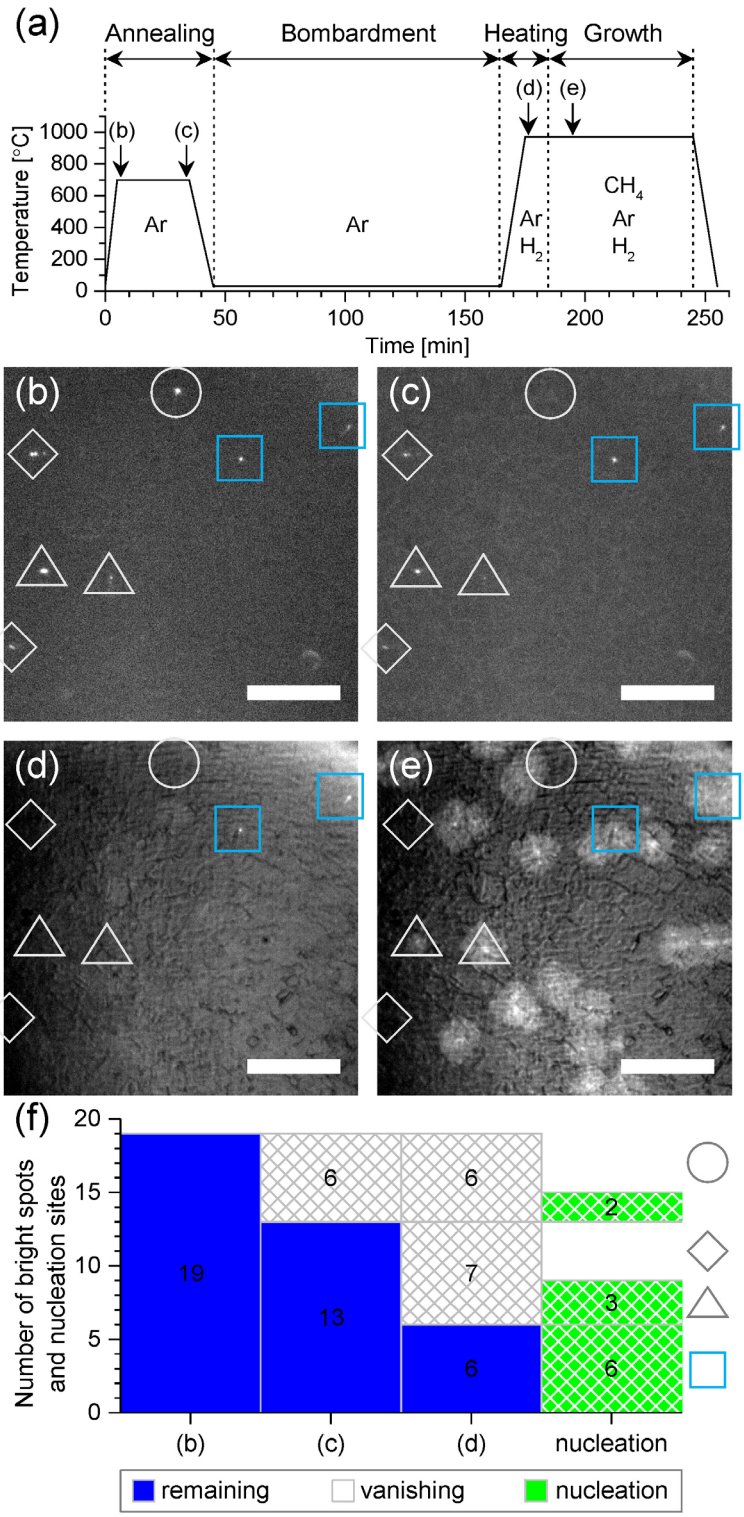


Figure 1.2 (a) Experimental sequence: annealing in Ar, Ar bombardment, heating to growth temperature, and growth. (b)–(e) Rad-OM images of the same Cu substrate at the times shown in (a). Circle, diamond, triangle, and square classify each bright spot as explained in the text. Scale bars: 500 μm. (f) The number of bright spots at the times of (b)–(e) and the relation between the nucleation site and each bright spot. The figure in each box means the number of bright spots remaining or vanishing at each step of the process and the number of nucleation sites. [34] Copyright (2017) The Japan Society of Applied Physics.

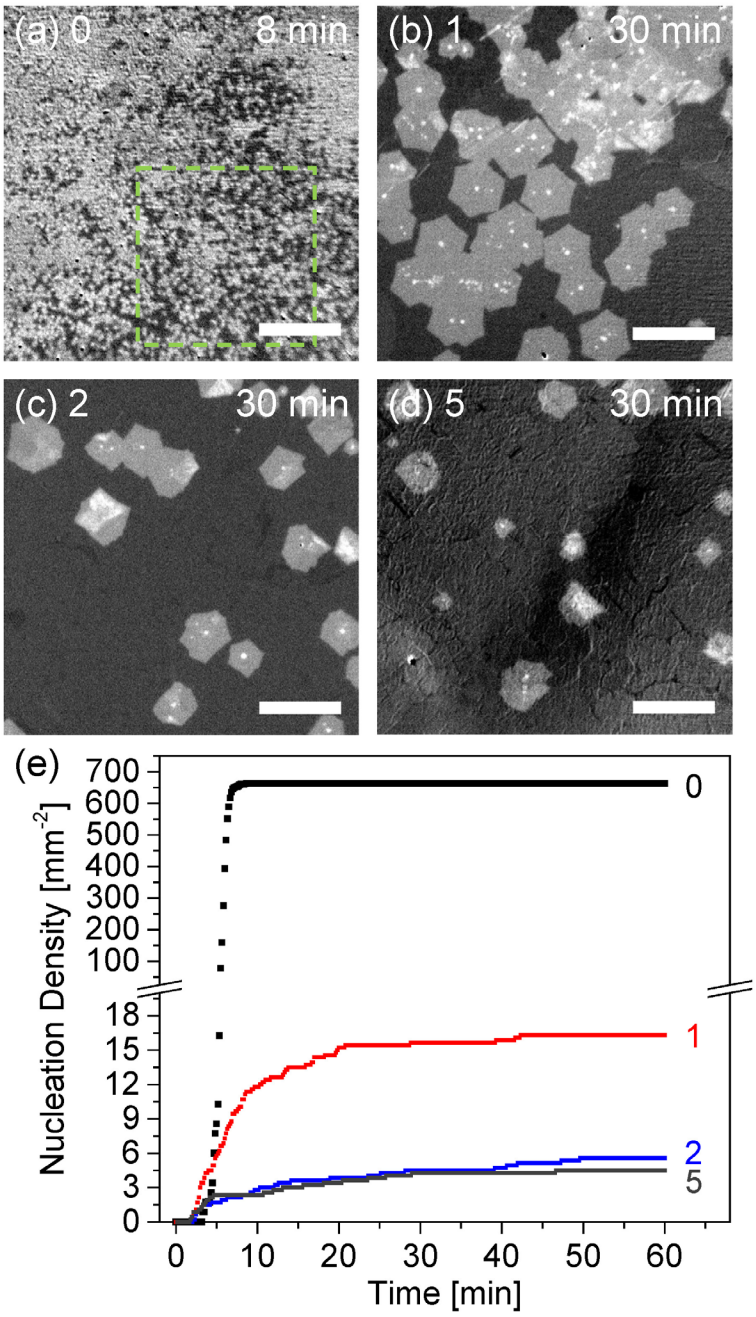


Figure 1.3 Rad-OM images of graphene growth after (a) Ar annealing, (b)–(d) one, two, and five cycles of Ar annealing and bombardment. The images were taken at (a) 8 min, (b)–(d) 30 min after the start of $CH_4$ supply. The white areas correspond to graphene grains. Scale bars: 500 μm. (e) Time evolution of graphene nucleation density. Black, red, blue, and gray dots indicate the nucleation density of the growths shown in (a), (b), (c), and (d), respectively. The figures denote the number of bombardments. Nuclei were counted within a green dashed square in (a), and within the entire image area in (b), (c), and (d). [34] Copyright (2017) The Japan Society of Applied Physics.

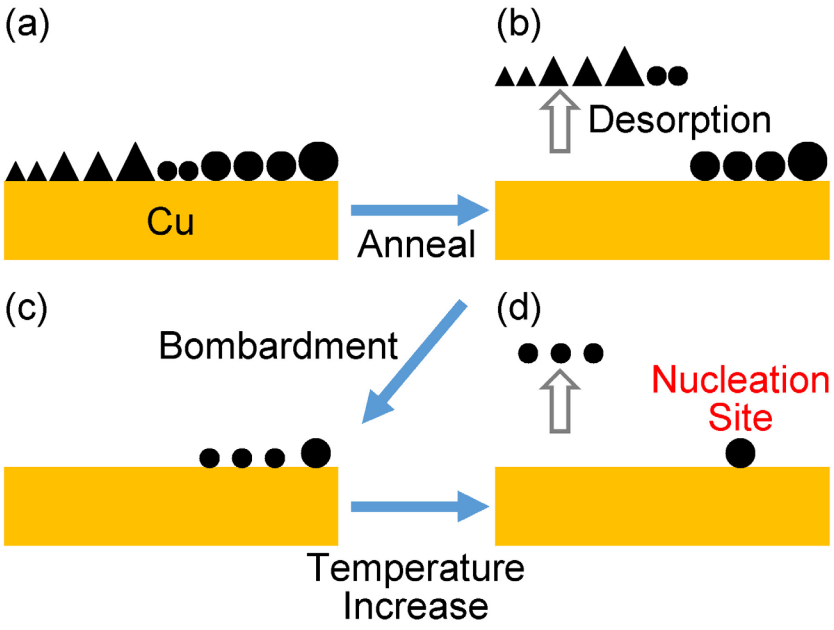


Figure 1.4 Schematic illustration of the behavior of carbon impurities on a Cu foil. (a) Volatile (triangle) and nonvolatile (circle) carbon impurities of various sizes exist on an untreated Cu substrate. (b) Annealing desorbs volatile impurities and small nonvolatile impurities. (c) Ar bombardment shrinks the size of the residual impurities. (d) Heating to growth temperature desorbs the small impurities. Initially large impurities still remain on the substrate and act as graphene nucleation sites. [38] Copyright (2017) The Japan Society of Applied Physics.

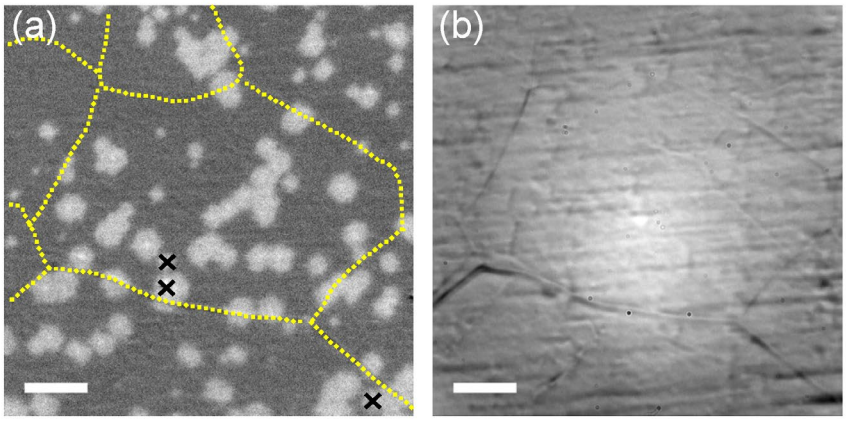


Figure 1.5 Nucleation sites of graphene domains on Cu foil with GBs: (a) Rad-OM image and (b) reflection image. The white areas in the Rad-OM image correspond to graphene domains. GBs are observed in the reflection image, which are represented by dashed lines in the Rad-OM image. The crosses show the graphene domains nucleated from the bright spots, which had been observed before the growth. Scale bars: 50 μm. [38] Copyright (2017) The Japan Society of Applied Physics.

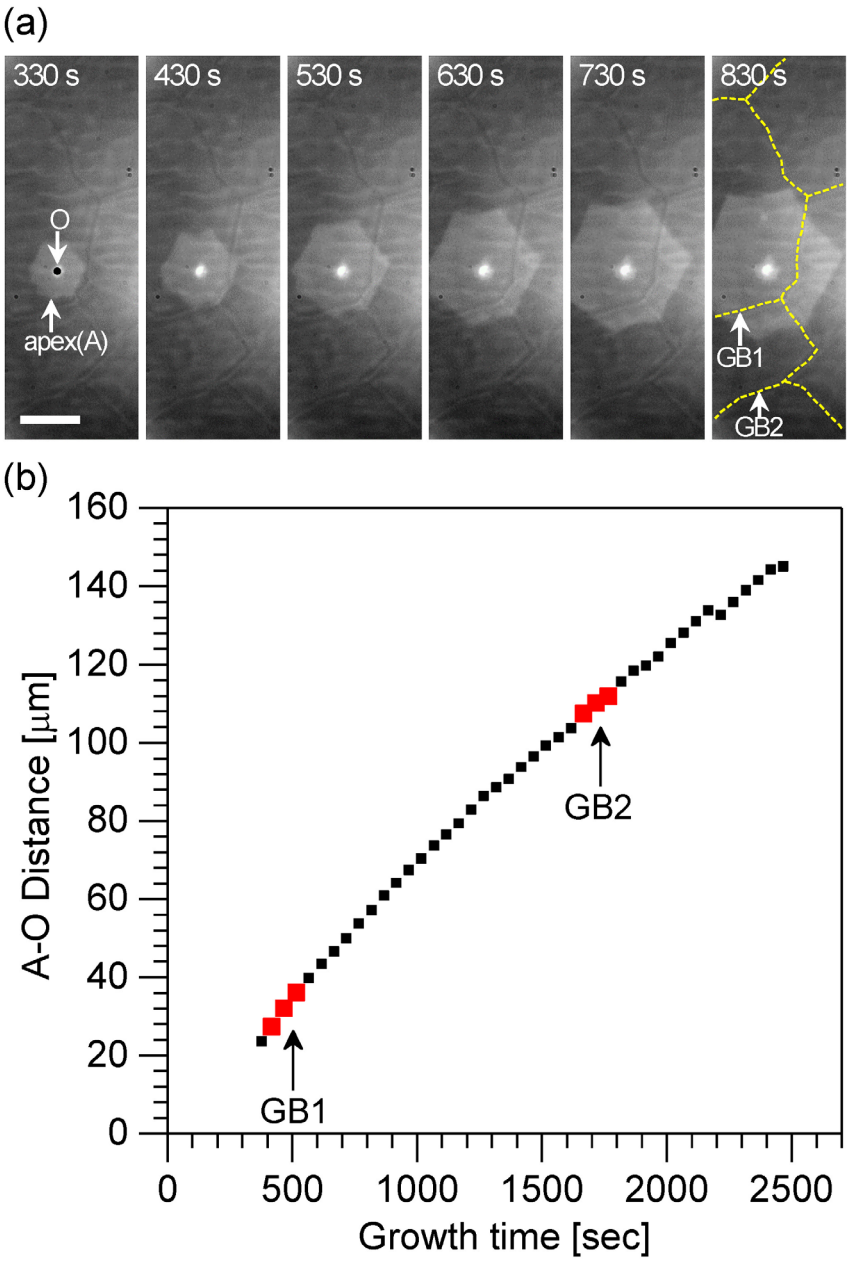


Figure 1.6 Evolution of a graphene domain on Cu foil. (a) Rad-OM images of the growing graphene domain 330, 430, 530, 630, 730, and 830 s (left to right) after the CH4 supply. The GBs are represented by dashed lines in the rightmost image. Scale bar: 50 μm. (b) Change in the distance between the center of the hexagon O (nucleation site) and the bottom-left apex A as a function of time after the CH4 supply. The time at which the apex A crossed the GB is indicated by an arrow. [38] Copyright (2017) The Japan Society of Applied Physics.

### 1.3.2. Gas parameters

The type of source gas, ratio of the gases including oxygen and hydrogen, decomposition of the source gas, and flow path of the gas were investigated as the gas parameters.

As one of the source gases, $CH_4$ is considered to be the best for low nucleation density because of its thermal stability compared to $C_2H_2$, $C_2H_4$, $C_6H_6$, and others [23], [25], [40], [41].

Lower $CH_4$ concentrations were more favorable for lower nucleation density because of a decrease in the amount of carbon on the substrate [39].

Introducing oxygen during annealing as the pretreatment or during growth suppressed nucleation by removing carbon impurities and graphene domains on the substrate [33], [42] and accelerated growth by decomposing $CH_4$ [40]. Oxygen impurities in Ar or $H_2$ were also reported to suppress nucleation [43], [44].

Hydrogen is generally supplied with $CH_4$ and Ar onto a Cu substrate. Various and sometimes conflicting effects of hydrogen have been reported; therefore, the major effect remains unknown. Several studies have reported that hydrogen suppressed nucleation [45]–[48], whereas others have reported that it induced nucleation [49]–[52]. Some studies have reported that hydrogen etched graphene [46], [53], [54], while others have reported that high-purity hydrogen did not etch graphene [55], [56]. In the present study, I investigated the effect of hydrogen on the CVD growth of graphene as described in Chapter 4.

Decomposition of the source gas by plasma (plasma CVD) or heated filament (hot-filament CVD) before the gas reaches the substrate was proposed. Plasma CVD was effective for graphene synthesis at low substrate temperatures [57], and hot-filament CVD affected the number of layers [58]–[60], quality [58], [59], [61], and crystallinity [62], [63] of graphene. Although it may accelerate growth, its actual effects on nucleation and growth remain unclear. Thus, I investigated the effect of the hot filament on the CVD growth of graphene as described in Chapter 3.

In addition, the gas flow paths affect the nucleation and growth rate. Cu foil folded into a pocket suppressed nucleation by Cu vapor or the formation of the molecular flow

of $CH_4$ inside the pocket [64]–[66]. The distribution of nucleation was also affected by the gas flow path [32].

### 1.3.3. Achievements and challenges of the optimization of parameters

The above parameters have been optimized in several studies and the synthesis of large-area single-crystalline graphene and its rapid growth were reported. For example, the 1 cm domain was synthesized via oxygen introduction [42], the 1.5 in. domain was obtained in 2.5 h by local $CH_4$ feeding onto a Cu-Ni alloy substrate [67], and 0.3 mm domain was obtained in 5 s by oxygen feeding from the oxide substrate [68].

However, I consider that presenting the optimized growth conditions is not sufficient for optimization of growth because growth is also affected by parameters specific to the growth chamber, such as the gas flow path, and the growth parameters must be optimized for each chamber. Therefore, establishing guidelines for optimizing parameters is a very important issue. For this purpose, it is necessary to elucidate how each parameter impacts the CVD growth of graphene.

## 1.4. Methods for the evaluation of the CVD growth of graphene

To elucidate the effect of each parameter, a quantitative in-situ evaluation of the CVD growth of graphene is required. Most previous studies were based on ex-situ observation, that is, the evaluation of graphene outside the growth chamber after growth has been completed. Nucleation density, size, growth rate, and the shape of the domains are typically observed by optical microscopy [69] or scanning electron microscopy (SEM) [23], and the quality of the graphene is mainly evaluated using Raman spectroscopy [70].

Ex-situ observation after completion of CVD growth does not provide adequate information to determine the effects of the various parameters on nucleation and growth. Ex-situ observation cannot accurately evaluate nucleation density because it is difficult to distinguish a single domain from domains that coalesced with each other during the early stage of the growth [71]. The evaluation of growth rate from the size of the grown domain is not precise because the nucleation time varies for each domain and the size of the domains is not uniform. In addition, ex-situ observation is affected by oxygen or carbon impurities in the air.

Thus, in-situ observation of the CVD growth of graphene is required to better understand the effects of the parameters. For this purpose, Rad-OM was developed by Terasawa and Saiki [72], [73]. Figure 1.7 depicts a schematic illustration of the underlying principle of Rad-OM. This method can visualize the CVD growth of graphene in real time by utilizing the difference in the emissivity of radiation light between graphene and Cu. It can also visualize the substrate morphology at the same location on the substrate by illuminating the substrate in a similar manner as in general optical microscopy (reflection-mode optical microscopy). Using Rad-OM, the effects of $CH_4$ flow rate and substrate temperature on the growth rate of graphene [73], the effect of oxygen on growth [74], and the growth of graphene on Au substrates were precisely evaluated [75]. In previous studies, I also used Rad-OM to investigate the effect of carbon impurities on nucleation [34] and the effect of GBs in Cu foil on nucleation and growth [38].

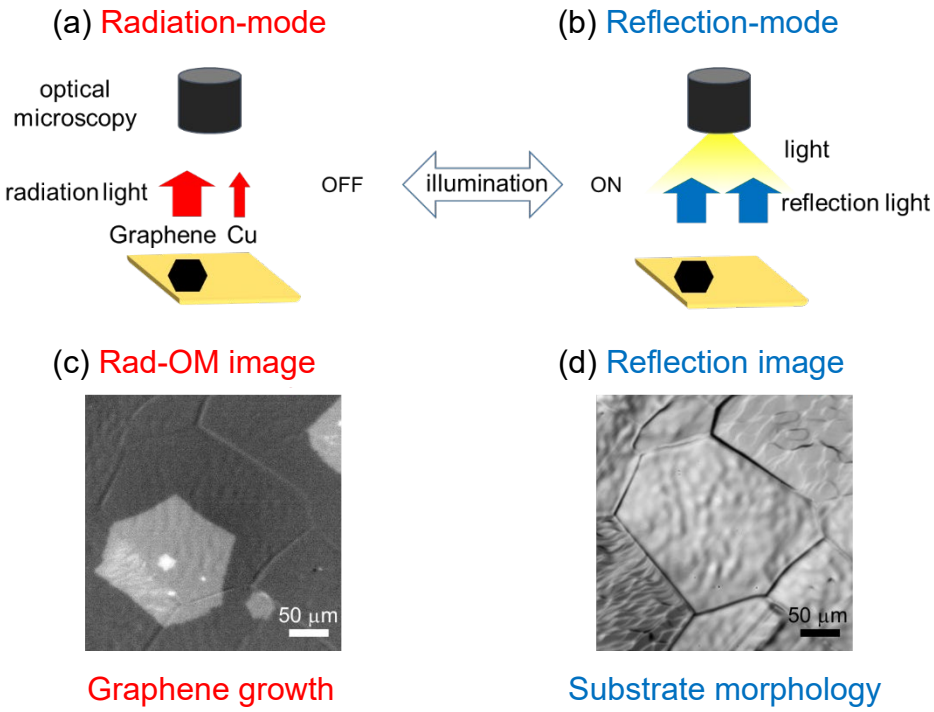


Figure 1.7 Schematic illustration of (a) radiation-mode and (b) reflection-mode optical microscopy, and examples of the (c) Rad-OM image showing graphene growth and (d) reflection image showing substrate morphology.

# 1.5. Purpose of this research

In this dissertation, I investigated two challenges associated with the CVD growth of graphene: (1) the effect of the hot filament and (2) the effect of hydrogen. The effects were elucidated by in-situ observation.

Hot-filament-assisted CVD (HF-CVD) decomposes the source gas using a high-temperature filament before the gas reaches the substrate. Although the hot filament is a potential candidate for growth acceleration, its effects on nucleation and growth are unclear. These effects were investigated using Rad-OM.

Hydrogen is generally supplied with $CH_4$ onto a Cu foil substrate. Various effects of hydrogen on the nucleation, growth, and etching of graphene during CVD growth were reported. Some of the effects were inconsistent with others; therefore, the major effect remains unknown. The effect of hydrogen was evaluated by changing the $H_2$ flow and observing the nucleation, growth, and etching of graphene by Rad-OM. Furthermore, Rad-OM and in-situ synchrotron radiation X-ray photoelectron spectroscopy (SR-XPS) were combined to characterize the surface species and evaluate the effect of hydrogen during growth and annealing.

# Chapter 2. Experimental

In this chapter, the principles, equipment, and the procedures for Rad-OM, XPS, and Raman measurements, and the experimental setup and the procedures for the CVD growth of graphene are explained. Further, the setup for the combined Rad-OM and in-situ SR-XPS measurements, which was developed in this study, is detailed.

## 2.1. Experimental principles

### 2.1.1. Radiation-mode optical microscopy (Rad-OM)

Rad-OM visualizes the CVD growth of graphene using the difference in the emissivity of radiation light between graphene and Cu. At the growth temperature (~1000 °C), substances emit radiation light according to Planck's law, which is termed black body radiation. The emissivity of radiation light at a specified temperature varies for each substance. The emissivities of graphite and Cu were 0.8 [76] and 0.03 [77], respectively. Thus, observation of radiation light with the optical microscope revealed the graphene domain as a brighter area and Cu as a darker area during CVD growth, as shown in Figure 1.7. In addition, the area of multilayer graphene was observed brighter than that of monolayer graphene. Further, the substrate morphology can be visualized by illuminating the substrate (reflection-mode optical microscopy), as shown in Figure 1.7. The advantage of this method is that it enables the observation of CVD growth, even under high temperature and high pressure conditions [72], [73].

### 2.1.2. X-ray photoelectron spectroscopy (XPS)

XPS is the method for analyzing the electronic states of the substances. Photoelectrons are emitted from the surface of the sample when the sample is irradiated with X-rays. According to Einstein's theory of the photoelectric effect, the relationship of energy is expressed as equation (2.1):

$$E_{kin} = h\nu - E_b - \phi \tag{2.1}$$

where $E_{kin}$ is the kinetic energy of the emitted photoelectrons, $h\nu$ is the energy of the incident X-ray, $E_b$ is the binding energy of the electron in the sample, and $\phi$ is the work

function of the sample. The value of $E_{kin}$ is obtained by XPS measurement. When the values of $h\nu$ and $\phi$ are known, the value of $E_b$ is obtained from equation (2.1). The value of $E_b$ enables identification of the element because the value is unique to each element. Since the value of $E_b$ is slightly shifted by the chemical environment around the atom, the state of the atom can be analyzed by measuring this energy shift (chemical shift) [78].

### 2.1.3. Raman spectroscopy

Raman spectroscopy is an effective method for evaluating carbon materials including graphene. In Raman scattering, light with a different wavelength than that of light incident on a substance is scattered from a sample. The difference in wavelength between the two lights (Raman shift) corresponds to the energy of molecular vibration and lattice vibration of the substance. Raman spectroscopy measures the intensity of scattered light for each wavelength. In the Raman spectrum, the observed intensity is plotted as a function of the Raman shift.

In the Raman spectrum of graphene, G, D, and 2D (G′) bands are mainly used to evaluate the quality of graphene. The G band appears at 1580 $cm^{-1}$, which is derived from the $sp^2$ C-C bond in graphitic carbon. The presence of the G band indicates the presence of the $sp^2$ carbon lattice in the sample. The D band appears at 1350 $cm^{-1}$, which is derived from the defects in the carbon lattice. The peak intensity of the D band increases as the number of defects increases. The peak intensity ratio of the D band to the G band ($I_D/I_G$) is used to evaluate the quality of graphene. For the applications of graphene, it is desirable that the D band intensity remains below the detection limit. The 2D (G′) band appears at 2700 $cm^{-1}$, which is derived from the double resonance Raman scattering in graphene. The peak intensity of the 2D band decreases as the number of graphene layers increases. The peak intensity ratio of the 2D band to the G band ($I_{2D}/I_G$) is used to evaluate the number of graphene layers. The ratio is typically > 2 for monolayer graphene [79].

# 2.2. Experimental equipment

## 2.2.1. CVD chamber with Rad-OM

Figures 2.1 and 2.2 show photographs of a CVD chamber and an optical microscope. The vacuum chamber is equipped with a mechanical pump, a turbomolecular pump, mass flow controllers, a gate valve, a pressure gauge (Tokyo electronics, CC-10), electric feedthroughs for heating the sample and filament, and an ion gun. After sample loading, the chamber was evacuated to $3.0\times10^{-5}$ Pa by the mechanical and turbomolecular pumps in 16 h. The total pressure was measured by the pressure gauge. Prior to graphene growth, the turbomolecular pump was stopped while the mechanical pump was kept on. The gas flow rates were regulated by each mass flow controller, and the total pressure was adjusted by slightly closing the gate valve. Then, the sample was heated by direct current from a power supply (Agilent, 6672A) under Ar and $H_2$ atmosphere. This heating method (cold-wall setup) was adopted for the local heating of the sample and to prevent the wall of the chamber from heating and emitting radiation light, which can be hinder to to the observations of radiation light from the sample [72]. The temperature of the sample was measured by a radiation pyrometer (Chino, IR-AH or Minolta, TR-630) and adjusted by tuning the voltage of the power supply.

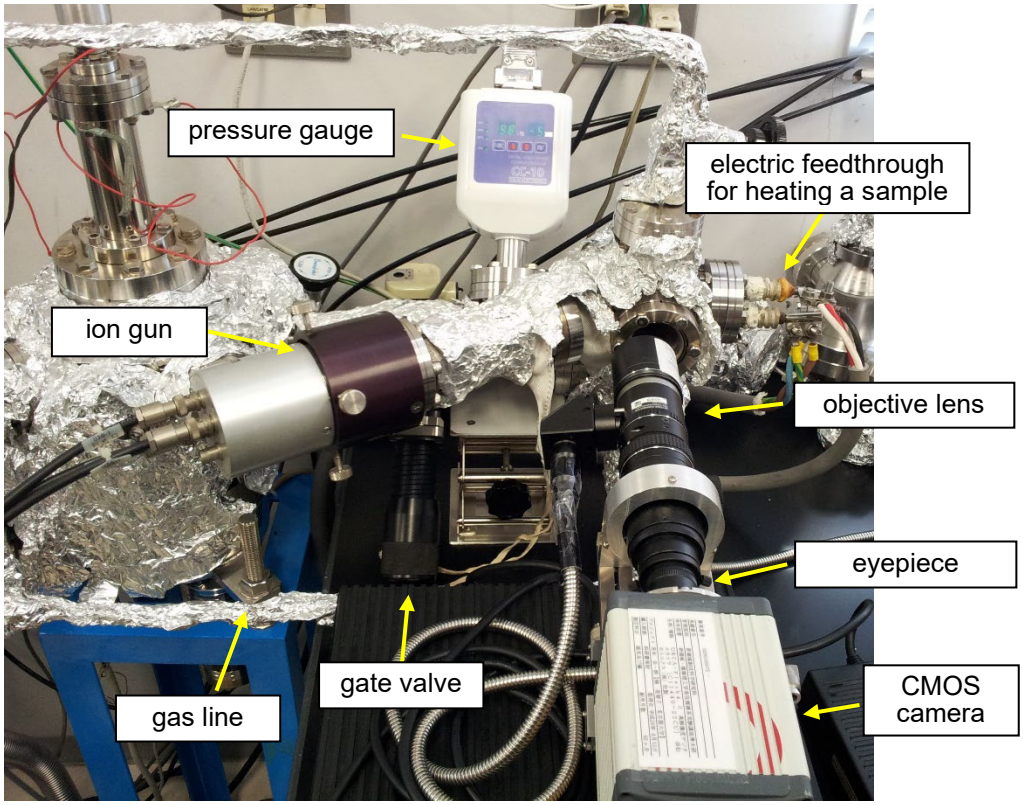


Figure 2.1 Photograph of the CVD chamber and an optical microscope in the laboratory.

A CMOS camera (Hamamatsu Photonics K.K., ORCA-Flash4.0 V2 C11440-22CU) with an objective lens (Keyence Co., VH-Z50L), an eyepiece (Optart, HRRC-4X), and a light (Moritex, MegaLight 100) was used as an optical microscope for in-situ observation of the CVD growth of graphene. The magnifications of the objective lens and eyepiece were ×500 and ×4, respectively. The position of the camera was adjusted by three microstages. Graphene growth at high temperatures was observed without the light (Rad-OM). The substrate morphology was observed with the light (reflection-mode optical microscopy).

During the observation, image data were acquired at 10 s intervals by a software HCImage Live (Hamamatsu Corporation) mainly with the following settings: exposure time = 100 ms, color depth = 16 bit. The observed area was 3.24 × 3.24 $\mu m^2$ and the acquired image was 1024×1024 pixels, so the size of a pixel was 316 × 316 $nm^2$ at the highest magnification.

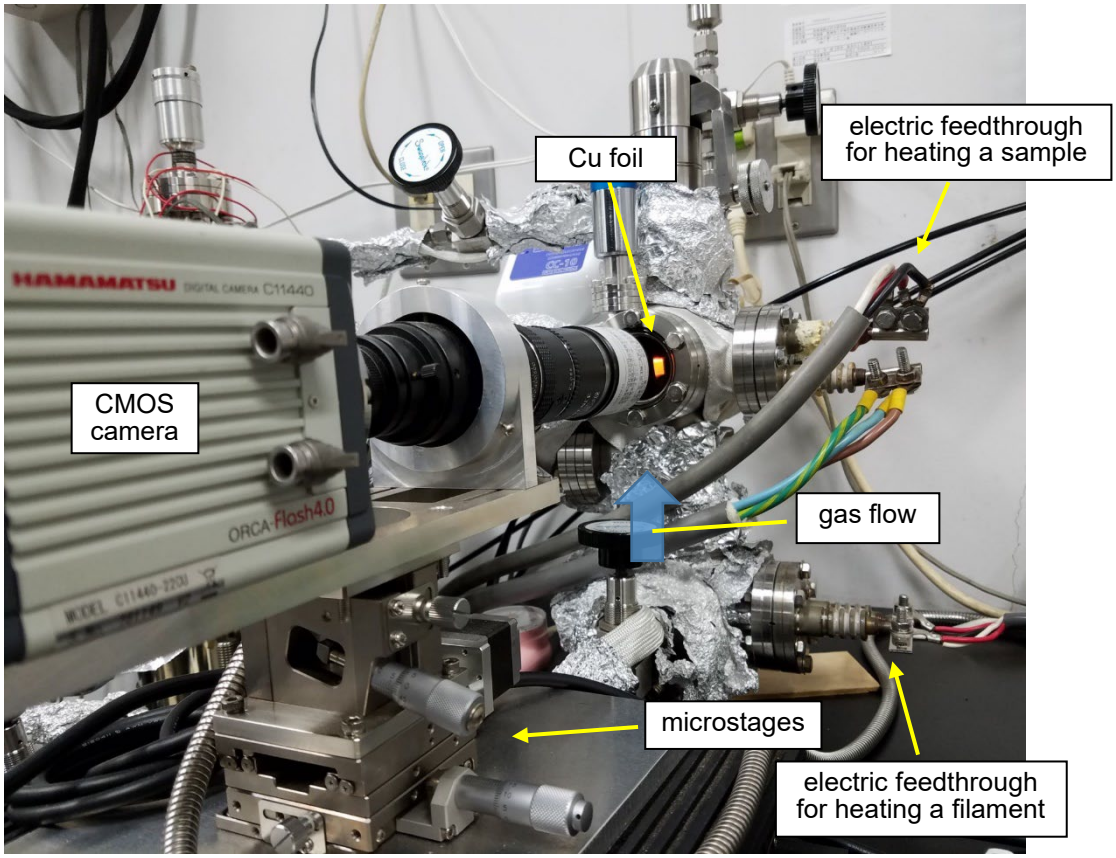


Figure 2.2 Photgraph of the CVD chamber during observation of graphene growth.

### 2.2.2. Synchrotron radiation XPS (SR-XPS) with Rad-OM

I combined Rad-OM observation with SR-XPS measurement at the High Energy Accelerator Research Organization, Photon Factory (KEK-PF) BL-13B. Figures 2.3 and 2.4 depict schematic illustration and photographs of the setup of Rad-OM with the SR-XPS chamber at KEK-PF BL-13B, respectively. The setup consists of three chambers: an XPS chamber (SES200), a preparation chamber, and a CVD chamber (load-lock chamber) with a heating station. Each chamber can be sealed to the other with gate valves. Samples can be transferred between each chamber with a transfer rod. The 10 cycles of annealing in vacuum and Ar bombardment were performed in the preparation chamber. CVD growth and annealing with $H_2$ were conducted in the CVD chamber and the processes were observed by Rad-OM. After the processes, the CVD chamber was evacuated and the sample was transferred to the XPS chamber to measure the substrate by XPS. The area of XPS measurement was about 210 μm (horizontal) × 40 μm (vertical) [80].

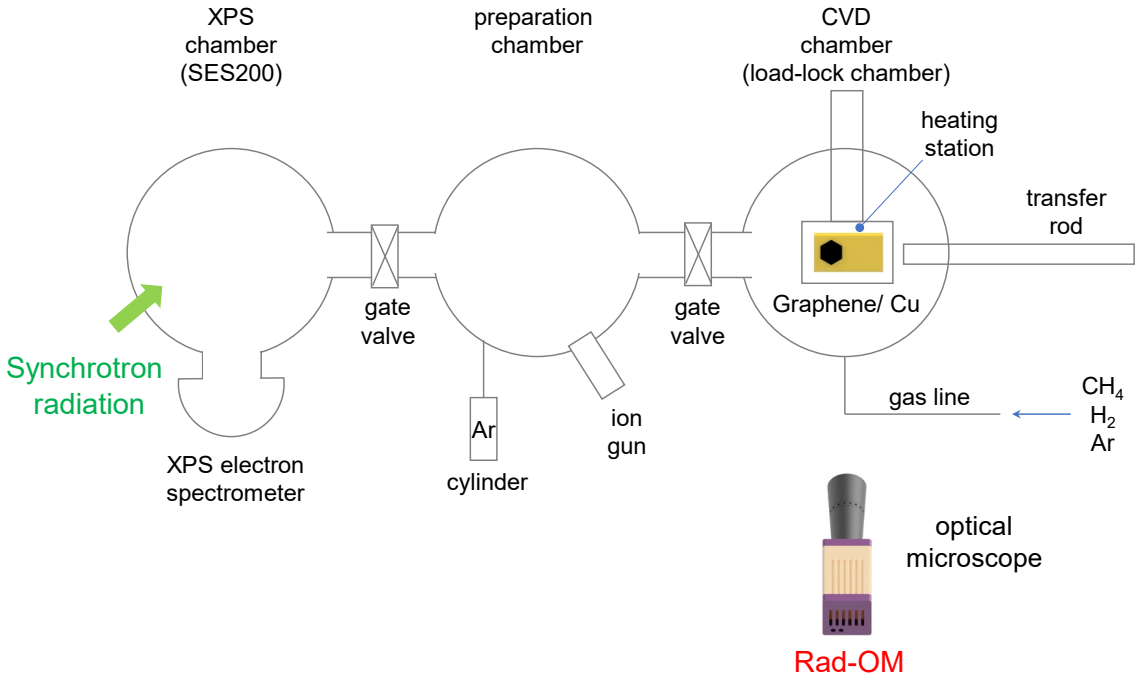


Figure 2.3 Schematic illustration of the setup of the SR-XPS and Rad-OM at KEK-PF BL-13B.

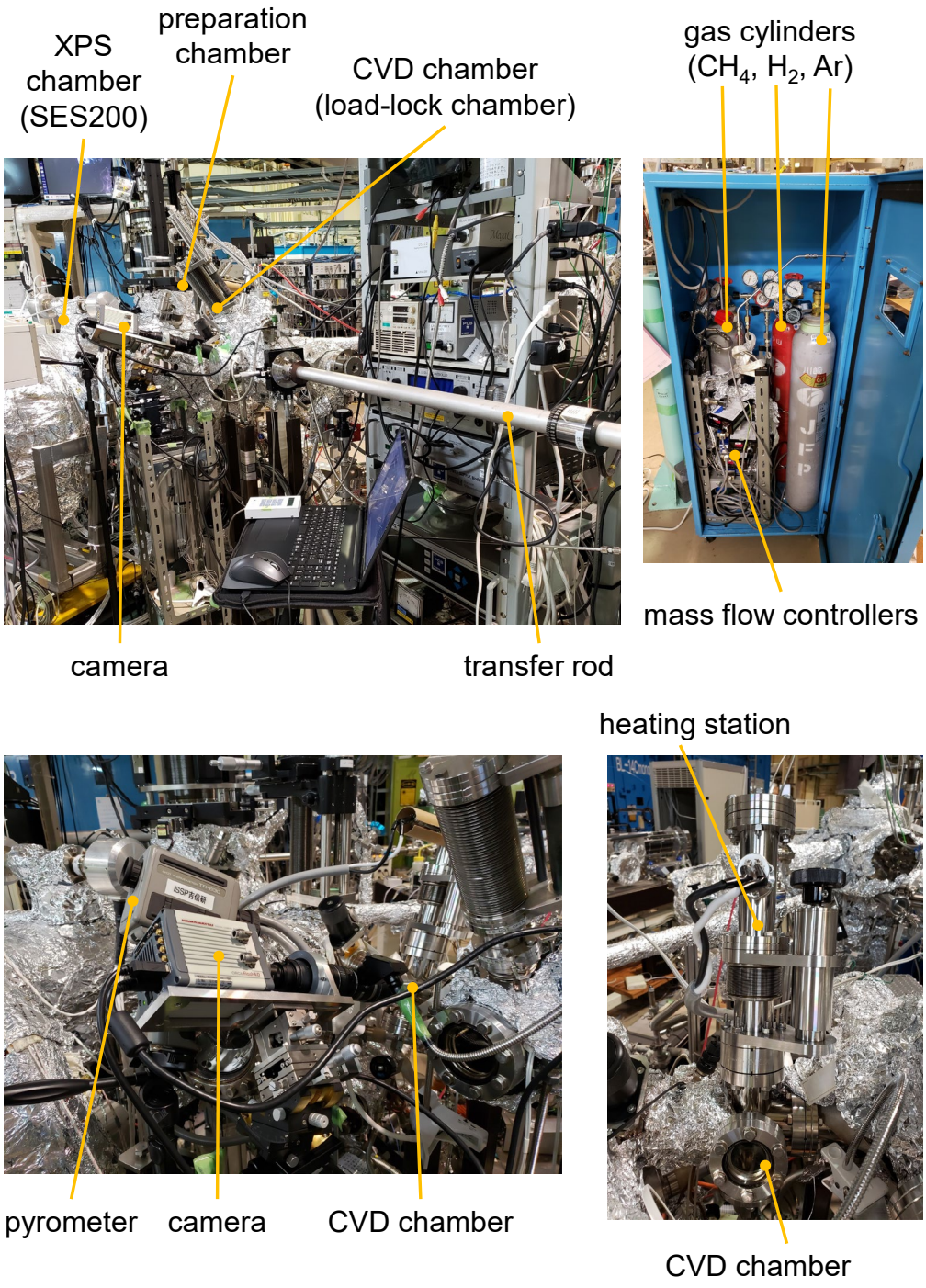


Figure 2.4 Photographs of the setup of the SR-XPS and Rad-OM at KEK-PF BL-13B.

To heat the Cu foil (3.2 × 3 $mm^2$) in the CVD chamber, I developed a heating station for heating, as shown Figure 2.5. When the sample holder is transferred to the heating station, an electric current passes through the electrode to the Ta foil and the Cu foil is heated. The heating station is attached to the CVD chamber as shown in Figure 2.4.

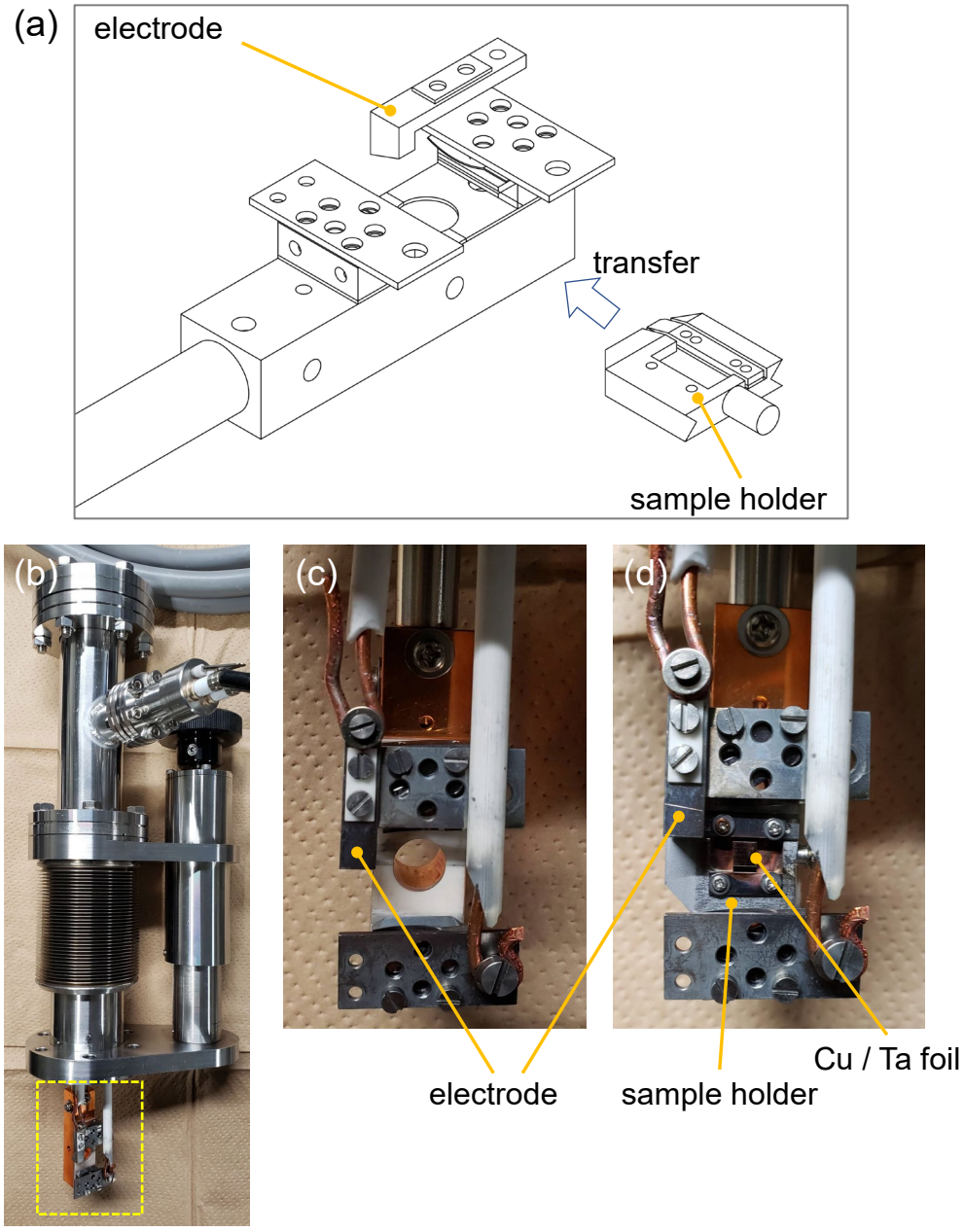


Figure 2.5 (a) Drawing and (b) photograph of the heating station.
(c), (d) Magnified photographs of the dashed rectangle in (b) when the sample holder is not transferred and transferred to the heating station, respectively.

### 2.2.3. Microscopic Raman spectroscopy

The quality of the synthesized graphene was evaluated using microscopic Raman spectroscopy (Renishaw, inVia Reflex), which consist of an optical microscope and a spectrometer (Figure 2.6). The measurement was conducted under the condition that the wavelength of the laser was 532 nm (Ar laser), the exposure time was 60 s, and accumulation was three times. The measurement area was ~1 μm in diameter.


Figure 2.6 Photograph of the equipment used in microscopic Raman spectroscopy.

# 2.3. Experimental procedure

## 2.3.1. Sample preparation

In the laboratory experiment, Cu foil (Rare Metallic, CU-88-83-230, purity: 99.99%, thickness: 50 μm) was used as a substrate, and W foil (Nilaco, W-463242, purity: 99.95%, thickness: 35 μm) or Ta foil (Nilaco, TA-413260, purity: 99.95%, thickness: 50 μm) was used as a heater. The W and Ta foils were used for the experiments described in Chapters 3 and 4, respectively. Figure 2.7 shows a method for preparing a sample. The Cu foil was cut into a size of 10 × 7 $mm^2$, and the W or Ta foil was cut into a size of 17 × 6 $mm^2$ (Figure 2.7(a)). The W or Ta foil was placed on the Cu foil (Figure 2.7(b)), and the Cu foil was bent to wrap the W or Ta foil (Figure 2.7 (c)). Figure 2.7 (d) shows the front observation side of the sample. Then, the Cu foil was pressed against the W or Ta foil to make the contact as uniform as possible. If the contact was not uniform, the temperature of the Cu substrate tended to be unstable when an electric current was passed through the W or Ta foil to heat the Cu substrate. Small pieces of the Cu foil were spot welded on both ends of the W or Ta foil to improve contact with the sample holder (Figure 2.7(a)). The sample was subsequently cleaned using an ultrasonic cleaner (As One, VC-1) in ultrapure water and acetone to remove the hydrophilic and hydrophobic impurities on the substrate, respectively (Figure 2.7(e)). After cleaning, the sample was dried with $N_2$ blow. Then, the sample was attached to the electrodes (Figure 2.7(f)) and loaded into a CVD chamber.

For the experiment at KEK-PF BL-13B, the Cu foil was cut into a size of 5 × 3 $mm^2$, and the Ta foil (Nilaco, TA-410173, purity: 99.95%, thickness: 10 μm) was cut into a size of 10 × 3.2 $mm^2$. The size of the sample was adjusted to the sample holder for the experiment at KEK-PF BL-13B. Then, the sample was pretreated in the same way as above and attached to the sample holder as shown in Figure 2.8.

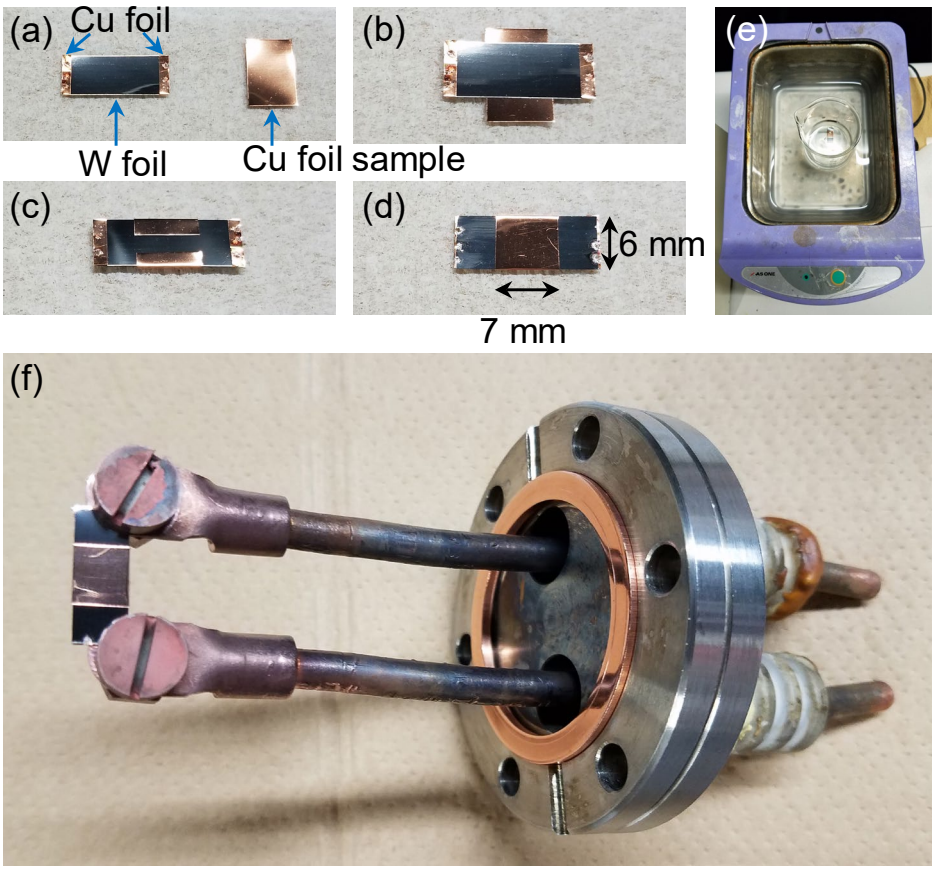


Figure 2.7 Photographs of the sample prepared in the laboratory. (a)–(d) Photographs of the different stages of sample preparation. (e) Ultrasonication of the sample. (f) Sample attached to the sample holder.

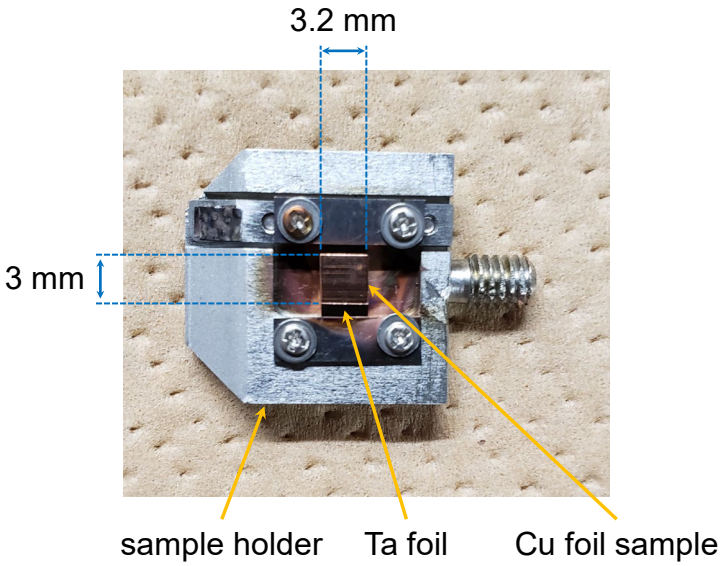


Figure 2.8 Photograph of the sample attached to the sample holder for the experiment in KEK-PF BL-13B.

### 2.3.2. CVD sequence

Figure 2.9 depicts the typical sequence of the entire process of pretreatment and CVD in the laboratory: annealing in Ar, Ar bombardment, heating to growth temperature, and graphene growth. First, the Cu foil was heated by passing an electric current through the W or Ta foil on which the Cu foil was placed, then annealed (700 °C, 30 min) in Ar (purity: 99.9999%, $O_2$ < 0.1 ppm) under a pressure of $5.7 \times 10^{-3}$ Pa. The temperature was set lower than the growth temperature to prevent the Cu evaporation under this low pressure. Next, Ar ion bombardment was conducted at room temperature (~25 °C) under a pressure of $5.7 \times 10^{-3}$ Pa with a beam voltage of 2 kV. The impinging ion current was typically 4 μA, which was spread over an area of 7 × 6 $mm^2$ on the Cu foil substrate. The pressure was adjusted to the condition of the operating environment of an ion gun (Ulvac, USG-3). After the pretreatment, a mixture of Ar and $H_2$ (purity: 99.99999%, $O_2$ < 0.02 ppm) gases was supplied and the total pressure was maintained at $1.0 \times 10^4$ Pa. The substrate temperature was then increased to 940 °C, and monitored for 10 min to confirm stabilization of the temperature. $CH_4$ (purity: 99.999%, $O_2$ < 1 ppm) was subsequently supplied to initiate graphene growth. After CVD growth, the $CH_4$ supply was stopped and the electric current was interrupted to cool the substrate to room temperature. The Ar and $H_2$ supplies were then stopped. The gas flow rates were systematically changed to evaluate their effects on graphene growth. During pretreatment and growth, the Cu foil was observed continuously by Rad-OM. The sample surface was observed by both Rad-OM and reflection-mode optical microscopy during annealing and heating, and was observed by Rad-OM during graphene growth.

Figure 2.10 depicts the typical sequence of the experiments conducted at KEK-PF BL-13B. First, 10 cycles of annealing (700 °C, 20 min) in vacuum and Ar bombardment ($6 \times 10^{-4}$ Pa, beam voltage: 0.5 kV, 30 min) were conducted in the preparation chamber. The substrate was subsequently measured by XPS to confirm the removal of carbon and oxygen impurities. CVD growth was conducted in the CVD chamber under the same conditions as that in the laboratory. The substrate was then observed by XPS. Thereafter, the substrate was annealed with $H_2$ in the CVD chamber to examine the effect of $H_2$ on graphene growth, and the substrate was then observed using XPS. During CVD and

annealing in the CVD chamber, the substrate was observed by Rad-OM.

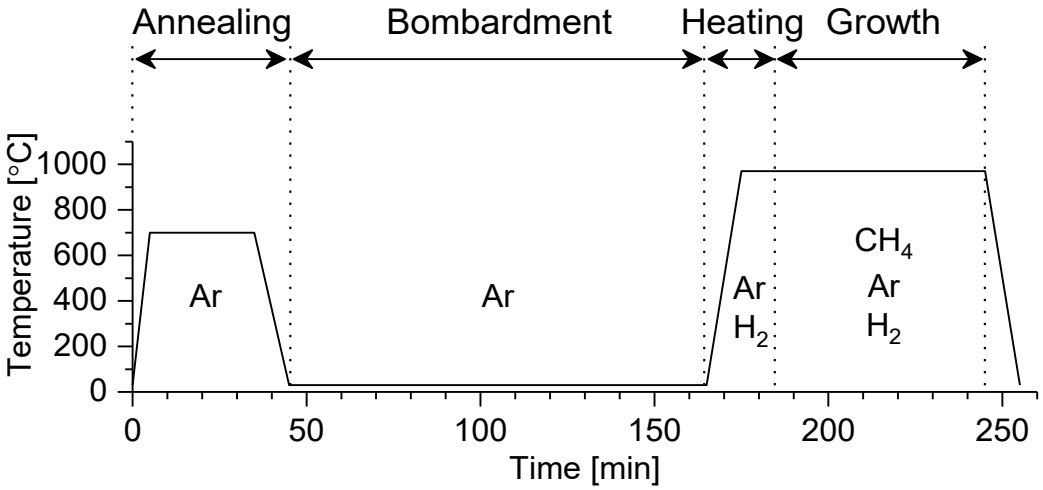


Figure 2.9 Typical sequence of pretreatment and CVD in the laboratory.

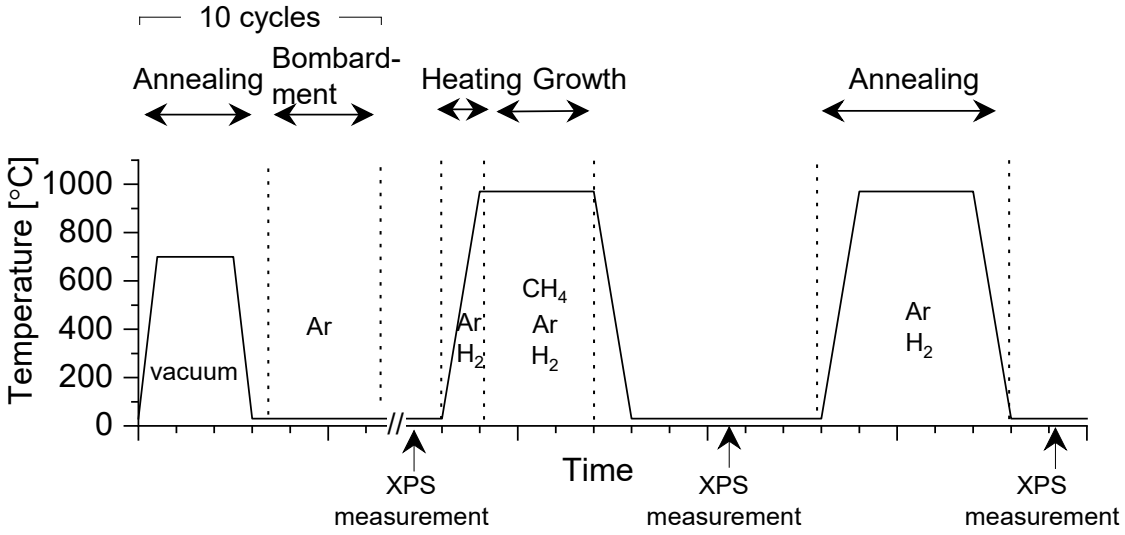


Figure 2.10 Typical sequence of pretreatment, CVD, annealing, and the XPS measurements at KEK-PF BL-13B.

### 2.3.3. Analysis of Rad-OM image

Acquired images by Rad-OM were processed using an open-source image processing software ImageJ. Typical images acquired by Rad-OM (Rad-OM image) were brighter at the center, as shown in Figure 2.11(a), which may be caused by lens aberrations. These background lights hinder the recognition of the graphene domains. To remove the background, the image at 0 s was subtracted from all Rad-OM images for the aberration correction, as shown in Figures 2.11 (b) and (c) [72]. After the background subtraction, Auto Contrast was applied to automatically adjust the image contrast, thereby making the images easily visible, as shown in Figure 2.11 (d).

The area of the graphene domain was analyzed by processing the Rad-OM image as follows: first, Gaussian Blur ($\sigma$=2) was applied to the Rad-OM image to reduce the noise. The images were then binarized, as shown in Figure 2.11(e): the pixels with higher and lower intensities than the threshold value were changed into white (intensity: 65536) and black (intensity: 0) pixels, respectively. The threshold value was determined by the Otsu algorithm. I tested all the built-in algorithms of ImageJ and visually estimated that Otsu was the best algorithm to distinguish areas of graphene from those of the Cu substrate. Finally, the area was recognized by Analyze Particles, a function of ImageJ. I visually estimated the nucleation time and shape of the domains because ImageJ experienced challenges in running them automatically due to noises when the size of the domain is small. The domain larger than 1 μm was recognized as the emergence of the domain.

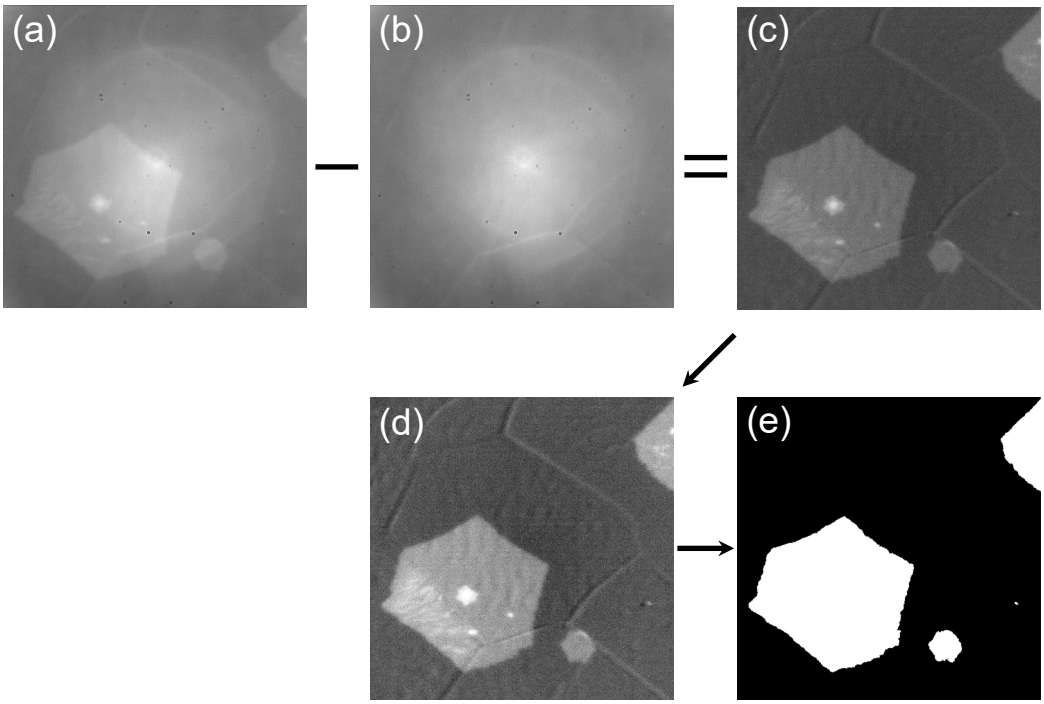


Figure 2.11 Example of image processing. (a) Example of a raw Rad-OM image. (b) Example of a raw Rad-OM image at 0 s. (c) Image made by subtracting (a) from (b). (d) Image after applying Auto Contrast to (c). (e) Binarized image of (d).

### 2.3.4. Measurement and calibration of XPS spectra

In the XPS measurement, the energy of the incident X-ray was set at 330 eV or 1100 eV. The Fermi edge of Cu was measured for each XPS measurement to convert the kinetic energy of the electrons into the binding energy of the electrons. Figure 2.12 shows an example of the XPS spectrum around the Fermi edge. The spectrum was fitted by following the Fermi distribution function (2.2), which indicates electronic state distribution near the Fermi level:

$$f(E) = \frac{1}{1 + \exp\left[\frac{E - E_f}{k_B T}\right]} \tag{2.2}$$

where $k_B$ is the Boltzmann constant, $T$ is temperature of the sample, and $E_f$ is Fermi energy. The Fermi energy ($E_f$) was obtained by fitting. Then, the kinetic energy of the electron was converted into the binding energy of the electron using the following relation (2.3):

$$E_b = E_f - E_{kin} \tag{2.3}$$

where $E_b$ is the binding energy and $E_{kin}$ is the kinetic energy of the electron [78].

The backgrounds of the XPS spectra differed for each measurement, as shown in Figure 2.13(a). The difference may be caused by the slight shifts in the position of the measurement by transferring the sample to the XPS chamber for each measurement. The intensity was calibrated by dividing the entire spectrum by the average intensity in a range of 1 eV (277.0 ± 0.5 eV in this example), as shown in Figure 2.13(b), based on the assumption that the background on the lower binding energy side of the peak should be equal. The peak fitting and calibration were performed using the software OriginPro.

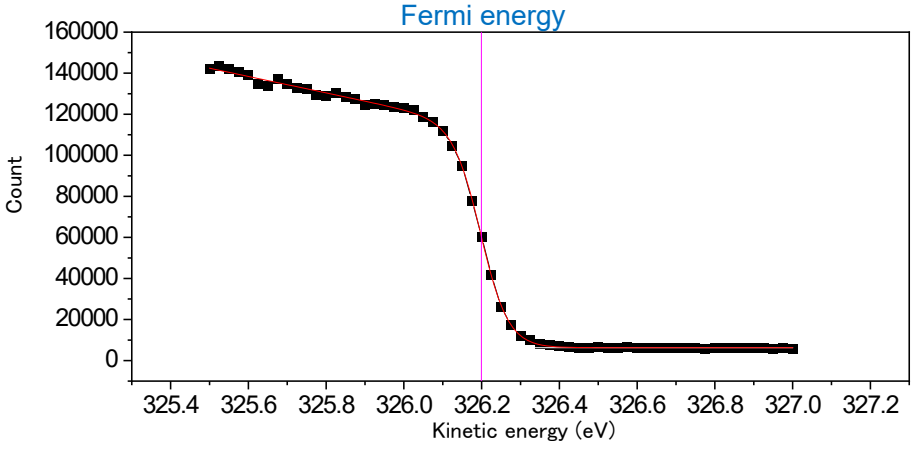


Figure 2.12 Example of the spectrum of the Fermi edge of Cu and its fitting to obtain the Fermi energy. hν=330 eV. T=300 K.

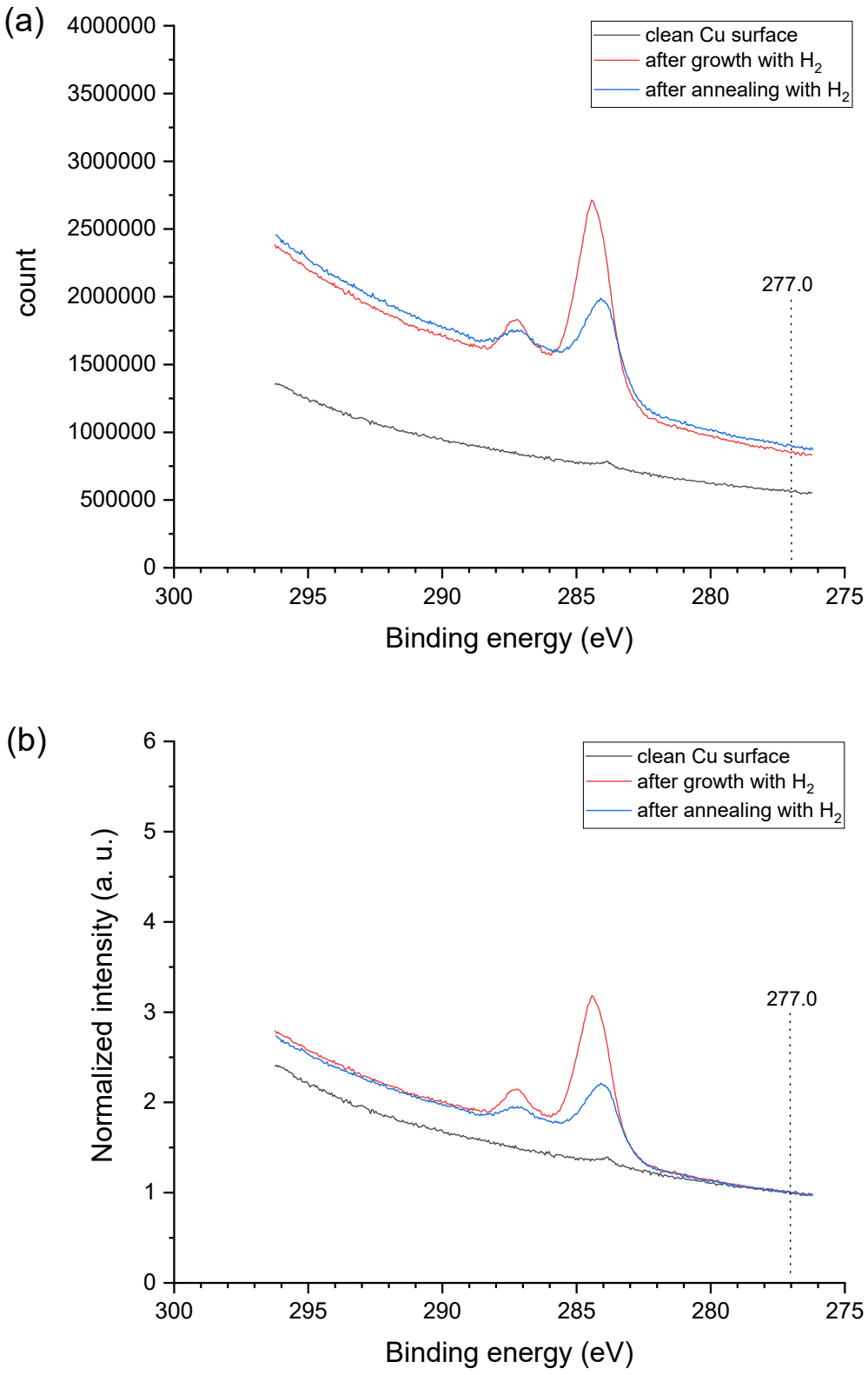


Figure 2.13 Example of the series of XPS measurements after the processes.
(a) Before and (b) after calibration of the intensity. The intensity was normalized at 277.0 ± 0.5 eV. hν=330 eV.

### 2.3.5. Measurement and analysis of Raman spectra

After CVD growth, the substrate was measured by ex-situ microscopic Raman spectroscopy at the same area as the observed area by Rad-OM according to the following procedure. During growth, the Rad-OM and reflection images were captured at the same location on the substrate, as shown in Figures 2.14(a) and 2.14 (b). After finishing growth, the substrate was removed from the chamber and observed by the optical microscope equipped with Raman apparatus. The area of graphene appeared slightly brighter, as shown in Figure 2.14(c) because the other area was slightly oxidized by the air [69]. By this contrast, the graphene domain observed by Rad-OM can be identified. Other areas can be identified by using the Cu GB as a landmark.

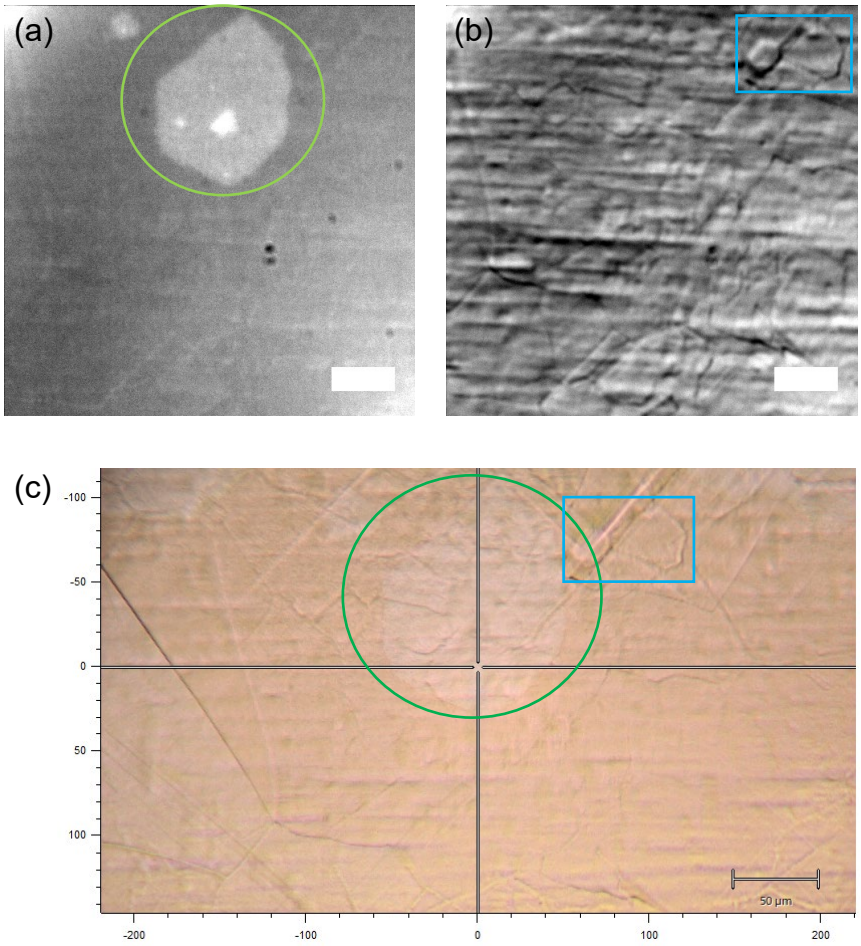


Figure 2.14 Examples of the (a) Rad-OM image and (b) reflection image during graphene growth at the same location on a substrate. (c) Optical image captured by an optical microscope equipped with Raman apparatus of the same substrate after the growth. The circles in (a) and (c) indicate the same graphene domain. The rectangles in (b) and (c) denote the same Cu GB. Scale bars: 50 µm.

# Chapter 3. Effect of hot filament

The effect of hot filament on the CVD growth of graphene was investigated using Rad-OM. The hot filament induced nucleation and accelerated graphene growth. These effects were enhanced by increasing the filament temperature. At a certain filament temperature (~1300 °C), growth was accelerated without additional nucleation. The present results suggest that the decomposition of source gas by the hot filament at optimized filament temperatures can accelerate the growth while suppressing additional nucleation. The use of the hot filament would be useful for rapidly synthesizing large-area single-crystalline graphene.

## 3.1. Introduction

Scalable and rapid synthesis of graphene is required for industrial applications. To rapidly synthesize large-area single-crystalline graphene by CVD, suppression of graphene nucleation and acceleration of growth should be simultaneously realized, as mentioned in Chapter 1. Various methods were developed to reduce the nucleation density and millimeter-sized graphene was achieved [42]–[44], [64], [81]–[84]. In most of the methods, the supply of source gases was reduced to suppress nucleation, which would simultaneously decelerate the growth. To solve this problem, various methods were examined, majority of which used complex processes such as local $CH_4$ feeding onto a Cu-Ni alloy substrate [67], oxygen feeding from oxide substrate [68], and so on [66], [85]–[89]. HF-CVD, in which source gases are decomposed by a high-temperature filament, is another potential candidate for growth acceleration. Although a few studies have examined the effect of the hot filament on the number of layers [58]–[60], quality [58], [59], [61], and crystallinity [62], [63] of HF-CVD-grown graphene, its effects on nucleation and growth remain unclear.

In this research, I investigated the effect of the hot filament on the nucleation and growth rate of graphene by Rad-OM. The results indicated that the hot filament induced nucleation and accelerated growth, which might be enabled by chemical species decomposed from $CH_4$ by a hot filament. Although these effects were enhanced by

increasing the filament temperature, only growth acceleration was observed at a certain temperature. These results imply that the hot filament at optimized temperatures will be effective for the rapid CVD growth of graphene with low nucleation density

# 3.2. Experimental

The details of Rad-OM are described in Chapter 2. The Cu foil (Rare Metallic, CU-88-83-230, purity: 99.99%, thickness: 50 μm, 10 × 7 $mm^2$) substrate was cleaned by ultrasonic cleaning in ultrapure water and acetone. Then, the Cu foil was wrapped around a W foil (Nilaco, W-463242, purity: 99.95%, thickness: 35 μm, 17 × 6 $mm^2$) and loaded into a chamber. Figure 3.1 depicts a schematic of the experimental setup. The Cu foil was heated by passing an electric current through the W foil, and the temperature of the Cu foil was monitored by a pyrometer from outside the chamber. A filament made of W was placed in the gas flow path before the Cu substrate. The W filament was heated by an electric current, and its temperature was monitored by a pyrometer.

Before graphene growth, the Cu foil was annealed at 700 °C for 30 min in Ar atmosphere under the pressure of 5.7 × $10^{-3}$ Pa. Then, Ar ion bombardment, which I proved to be effective for suppressing graphene nucleation [34], was conducted at room temperature with a beam voltage of 2 kV. The impinging ion current was typically 4 μA, which was spread over an area of 7 × 6 $mm^2$. After pretreatment, the mixture of 750 sccm Ar and 200 sccm $H_2$ gases was supplied with a total pressure of 1.0 × $10^4$ Pa. Then, the substrate temperature was maintained at 950 °C, and $CH_4$ was supplied to initiate graphene growth. The $CH_4$ flow rate was set at 1 sccm for the growth shown in Figures 3.2 and 3.3, and systematically changed for the growth shown in Figures 3.4 and 3.5.

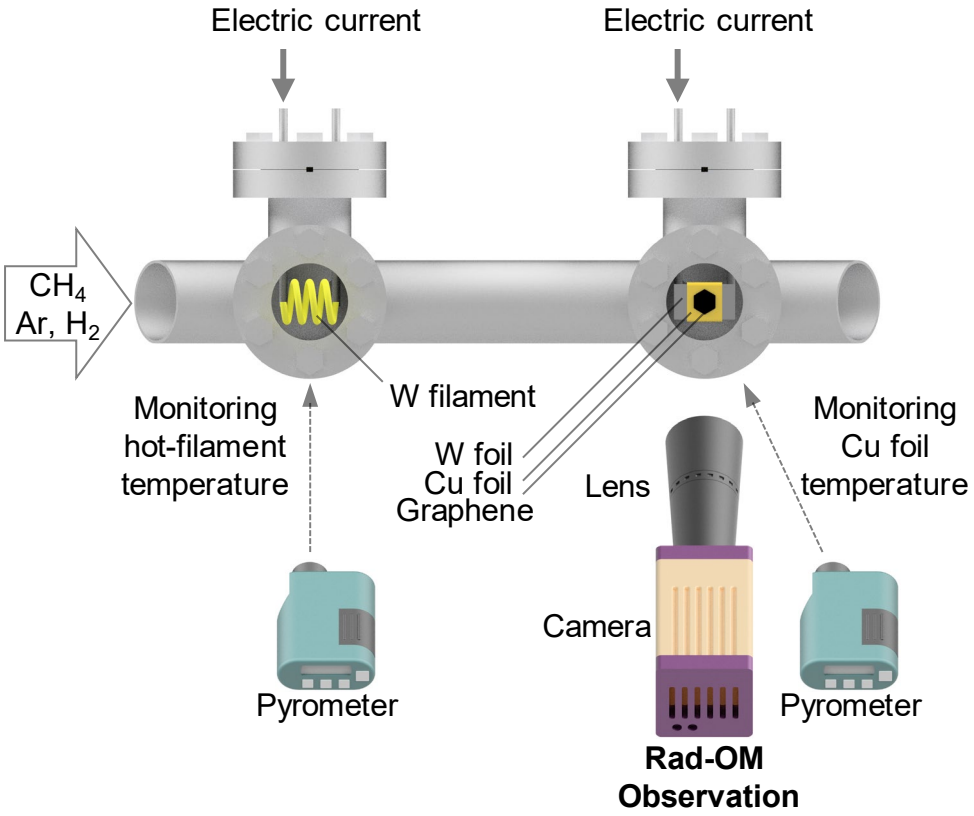


Figure 3.1 Schematic illustration of the experimental setup to examine the effect of the hot filament. [109] Copyright (2019) The Japan Society of Applied Physics.

# 3.3. Results and discussion

## 3.3.1. Effect on nucleation

To examine the effect of the hot filament on graphene nucleation, the filament current (temperature) was gradually increased during graphene growth under a $CH_4$ flow rate of 1 sccm. Figure 3.2 shows a sequence of the Rad-OM images cut from the Rad-OM movie. Before turning the W filament on, two graphene grains grew at an average rate of 2.4 μm/min (Figure 3.2(a)). After the W filament was turned on, the lateral growth continued without formation of additional grains, until the current was increased to 7.6 A (Figures 3.2(b) and 3.2(c)). However, when the current was increased to 7.8 A, new grains were observed (Figure 3.2(d)). When the current was set at 7.9 A, all grains grew at an average rate of 4.2 μm/min, but no more additional nucleation occurred (Figure 3.2(e)). After the current was increased to 8.1 A, the number of grains drastically increased (Figures 3.2(f)-(i)) and the grains grew further. The number of nuclei is plotted as a function of time in Figure 3.3.

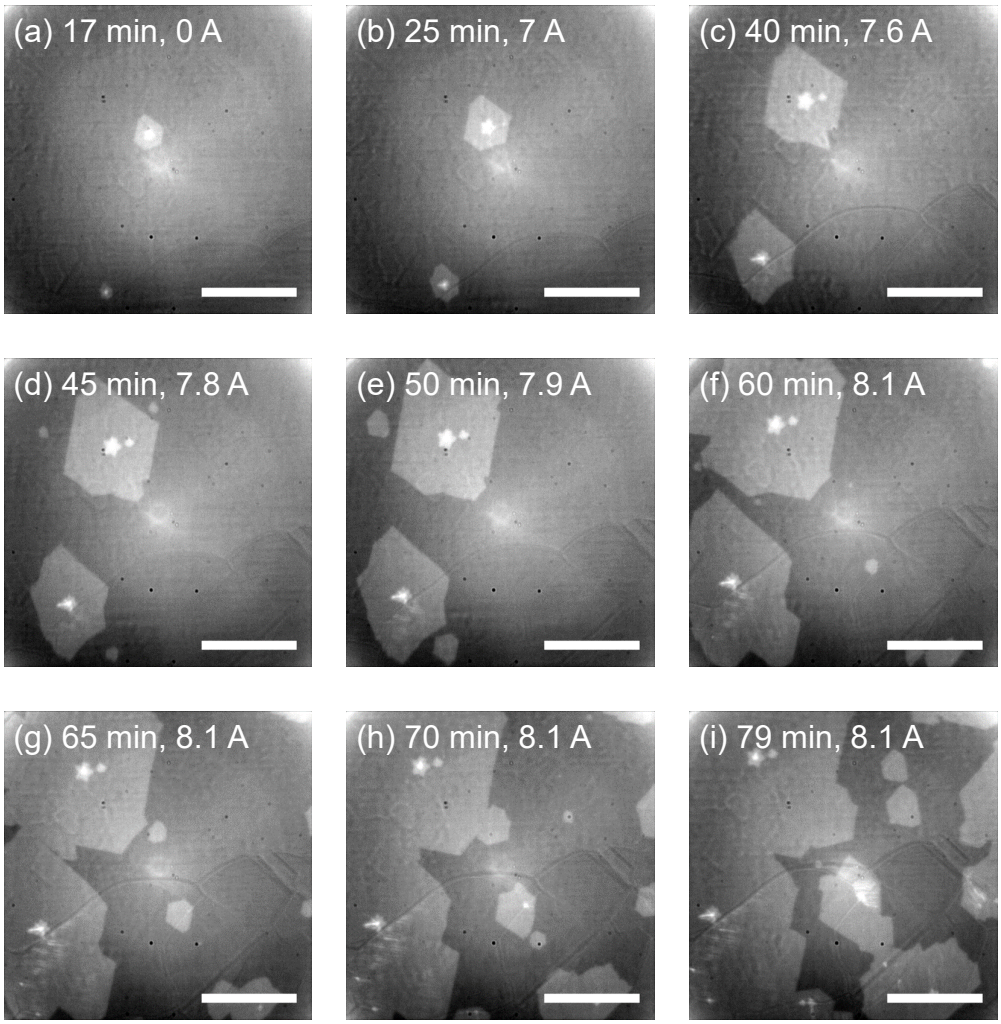


Figure 3.2 Rad-OM images of the graphene growth at growth times of 17, 25, 40, 45, 50, 60, 65, 70, and 79 min and filament current of 0, 7, 7.6, 7.8, 7.9, 8.1, 8.1, 8.1, 8.1 A, respectively. Cu substrate temperature was kept at 950 °C and $CH_4$ flow rate was set at 1 sccm. Growing areas correspond to graphene. Scale bars: 200 μm. [109] (Partially modified) Copyright (2019) The Japan Society of Applied Physics.

Figure 3.3(a) indicates the time evolution of the number of nuclei, which was counted from the same Rad-OM movie as Figure 3.2. The filament current, together with the corresponding temperature is shown in Figure 3.3 (b). When the filament temperature was < 1270 °C, the number of nuclei remained at 2. When the filament temperature was increased to 1270 °C, the number increased by 3, and remained constant at 5 until the filament temperature was further increased to 1340 °C. Then, after setting the filament temperature at ≥ 1340 °C, the number drastically increased by 15. These results indicate that the hot filament induced nucleation above a certain temperature (1270 °C in this condition), but did not induce nucleation below 1270 °C.

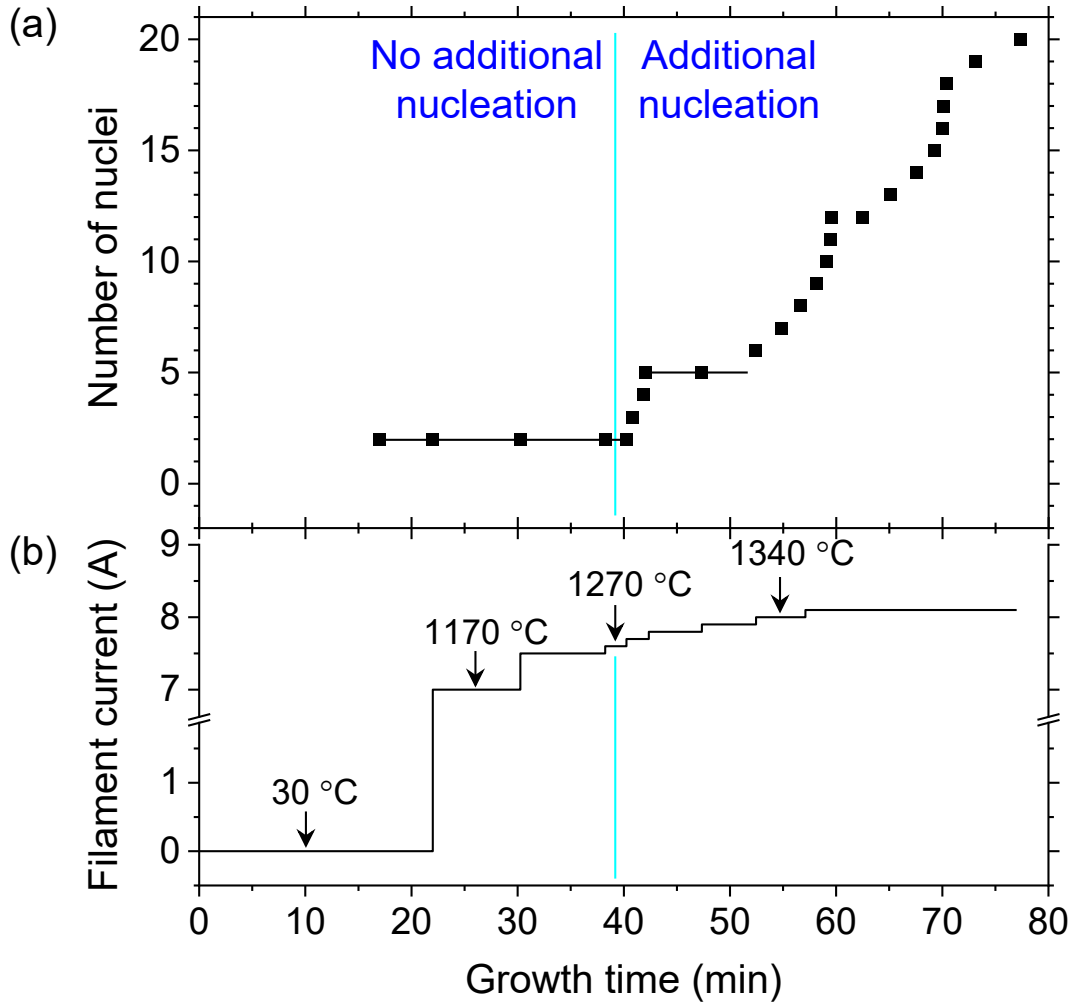


Figure 3.3 (a) Number of nuclei counted in the image of Figure 3.2. and (b) value of filament current as functions of growth time. A corresponding filament temperature is shown in the graph. Additional nucleation did not occur at the filament temperature below 7.6 A but occurred above 7.6 A. [109] (Partially modified) Copyright (2019) The Japan Society of Applied Physics.

Next, the critical flow rate of nucleation was investigated for growth with and without the hot filament. The temperature of the hot-filament was set at 1340 °C, which was expected to induce additional nucleation, as observed from the results in Figures 3.2 and 3.3. For each growth process, the $CH_4$ flow rate was increased by 0.1 sccm every 10 min to examine whether nucleation was induced by each $CH_4$ flow rate. Figures 3.4(a) and 3.4(b) show the Rad-OM images taken 10 min after each flow rate was set without and with the hot filament, respectively. Graphene first nucleated at 0.6 sccm (Figure 3.4(a)) and 0.4 sccm (Figure 3.4(b)), without and with the hot filament, respectively. Thus, the minimum $CH_4$ flow rate for graphene nucleation was decreased by the hot filament. When the hot filament was not used, the precursors for graphene nucleation were formed only on the Cu substrate maintained at 950 °C and the $CH_4$ flow rate had to be larger than 0.6 sccm for nucleation to occur. When the hot filament was used, the same amount of precursors was supplied at the $CH_4$ flow rate of 0.4 sccm. Furthermore, comparison of the grain size in the rightmost images of Figures 3.4(a) and 3.4(b) indicates that growth with the hot filament was faster than that without, even though the $CH_4$ flow rate of the former was lower than that of the latter. This difference in the growth implies that the hot filament can accelerate growth. Hence, next the effect of the hot filament on the growth rate was analyzed.

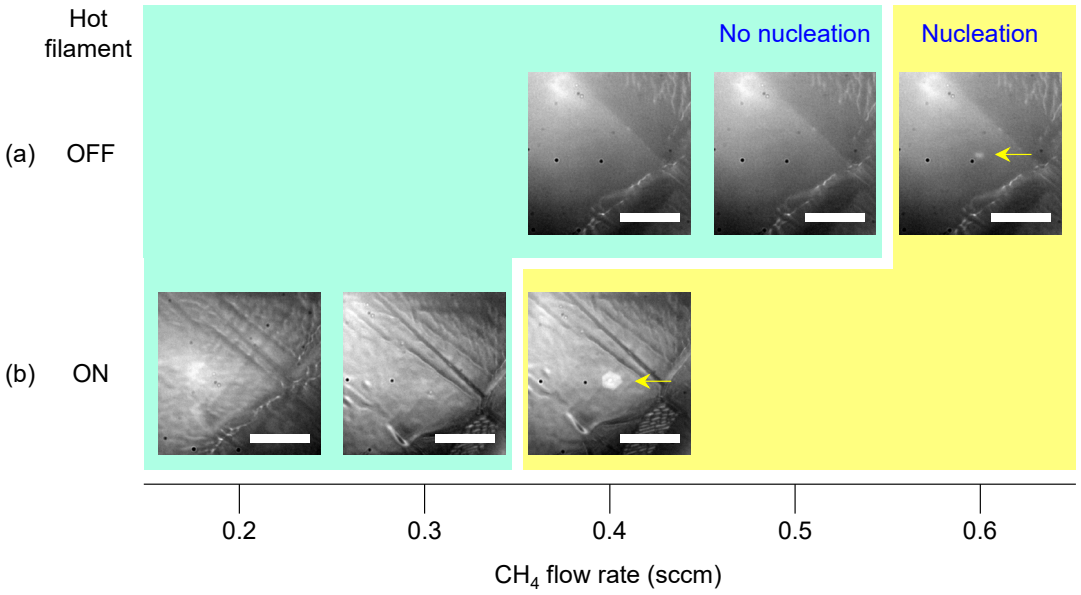


Figure 3.4 Rad-OM images of the graphene growth taken 10 min after setting each $CH_4$ flow rate (a) without and (b) with the hot filament at 1340 °C. Cu substrate temperature was maintained at 950 °C. Graphene nucleated at 0.6 sccm and 0.4 sccm without and with the hot filament, respectively. The arrow denotes the graphene grain. Scale bars: 200 μm. [109] Copyright (2019) The Japan Society of Applied Physics.

### 3.3.2. Effect on growth rate

The change in grain size was measured under various growth conditions of hot filament temperature and $CH_4$ flow rate to compare their effect on the growth rate. Figure 3.5(a) shows the Rad-OM images of the growth, and the grain size is defined as the distance between one apex and the center of the grain (nucleation site) [38], as indicated in the magnified image. After forming a few nuclei in the range of vision (405 × 405 $\mu m^2$), the $CH_4$ flow rate was maintained at 0.4 sccm. Under this condition, additional nucleation and lateral growth hardly occurred. At 37 min, the hot filament was turned on to set its temperature at 1740 °C. Then, based on the sequence shown in Figure 3.5(c), the filament temperature was decreased step by step, avoiding new grain formation. In Figure 3.5(b), the grain size measured from the Rad-OM movie is plotted, and the growth rate calculated from the gradient of the graph is displayed. As the filament temperature decreased, the growth rate decreased and became zero at 1130 °C. To compare the effect of the hot filament with that of flow rate, the $CH_4$ flow rate was increased stepwise after the hot filament was turned off at 82 min. The grain began to grow again, and the growth rate increased as the flow rate increased.

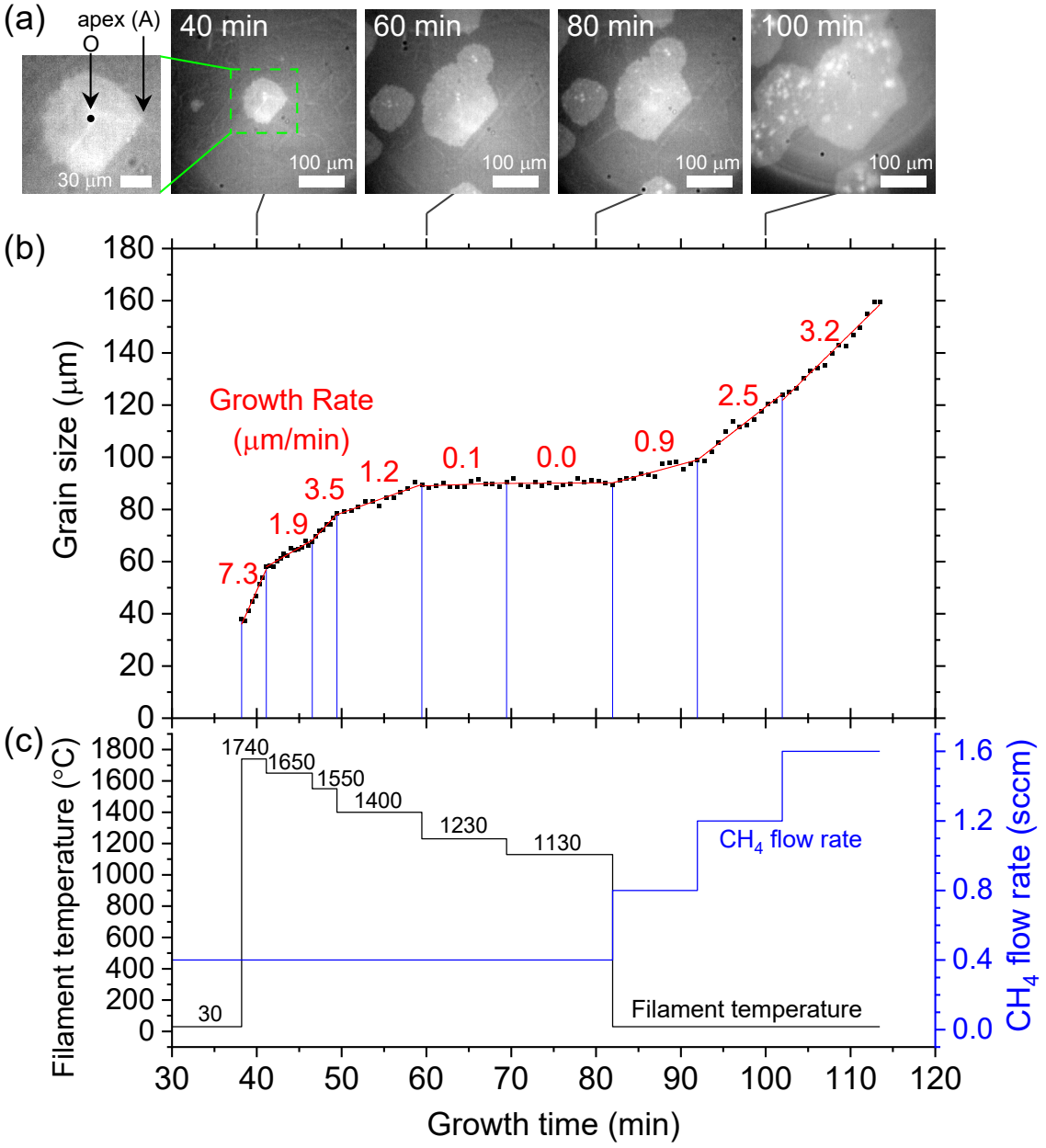


Figure 3.5 (a) Rad-OM images of the graphene growth taken at 40, 60, 80, and 100 min after $CH_4$ supply, and the magnification image of the image at 40 min. (b) Grain size and (c) filament temperature (left axis) and $CH_4$ flow rate (right axis) as functions of growth time. The Cu substrate temperature was maintained at 950 °C. Grain size is defined as the distance between a nucleation site O and a right apex A in (a). Growth rate is indicated in (b) for each condition. [109] (Partially modified) Copyright (2019) The Japan Society of Applied Physics.

The growth rate is plotted as a function of the filament temperature and $CH_4$ flow rate in Figure 3.6(a). After the filament was turned off, the growth rate increased almost linearly with the flow rate. Graphene did not grow for the 0.4 sccm $CH_4$ supply, so the threshold flow rate was ~0.5 sccm. However, graphene growth was observed for filament temperatures > 1230 °C, even at a $CH_4$ flow rate of 0.4 sccm; the growth rate increased dramatically with increasing temperature. In the pyrolysis of $CH_4$, $C_2H_2$ was observed above 1200 °C [90], [91]. These results imply the supply of $C_2$ species from the vapor phase in addition to that formed on the Cu substrate. This mechanism will be discussed in Section 3.3.3. The growth rate on a log scale is plotted as a function of the reciprocal temperature in Figure 3.6(b). For temperatures < 1550 °C, the relationship is almost linear and fitted to the Arrhenius equation (dashed line in Figure 3.6(b)). Using the slope of the fitted line, the activation energy was estimated at 4.7 eV. The gas-phase dehydrogenation of $CH_x$ to $CH_{x-1}$ ranges from 3.7 to 5.1 eV [92]. The activation energy shown in Figure 3.6(b) is considered to be this dehydrogenation energy [92].

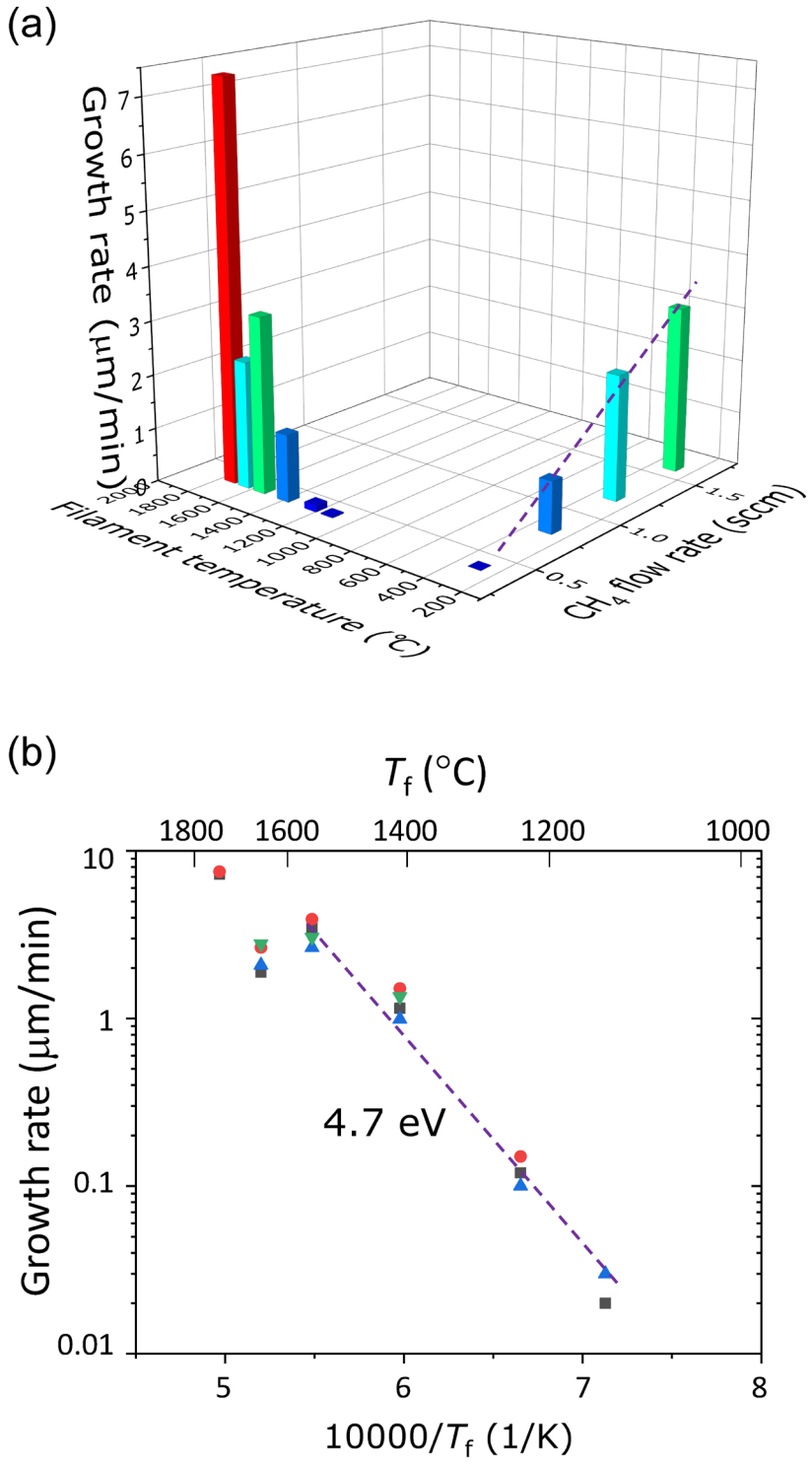


Figure 3.6 (a) Growth rate as a function of filament temperature and $CH_4$ flow rate. (b) Arrhenius plot for the growth shown in Figure 3.5. $T_f$: filament temperature. Growth rate was measured at 4 apices in Figure 3.5(a), and the average value and each value is plotted in (a) and (b), respectively. The dashed line denotes the relationship fitted to Arrhenius equation. [109] Copyright (2019) The Japan Society of Applied Physics.

### 3.3.3. Discussion of the effect of hot filament

The results indicated that the hot filament induced nucleation and accelerated growth, which were enhanced by raising the filament temperature. Notably, acceleration without additional nucleation occurred at a filament temperature of 1270 °C under the growth conditions shown in Figures 3.2 and 3.3. These results could be explained by the difference in the type and quantity of the chemical species generated by the hot filament and catalytic Cu substrate. Especially, the amount of $C_2H_2$, which is generated from the pyrolysis of $CH_4$ by hot filament, seems the key factor.

In the pyrolysis of $CH_4$ by hot filament, the $CH_4$ decomposition steps were suggested as (3.1):

$$\begin{aligned} 2\ CH_4 &\rightarrow C_2H_6 + H_2 \\ &\rightarrow C_2H_4 + 2\ H_2 \\ &\rightarrow C_2H_2 + 3\ H_2 \\ &\rightarrow 2\ C + 4\ H_2 \end{aligned} \tag{3.1}$$

The formation selectivity of $C_2H_2$ increases dramatically with increasing temperature in the range of 1200–1600 °C, because the formation rate of $C_2H_2$ is considerably higher than the decomposition rate of $C_2H_2$ [90], [91].

During CVD graphene growth, $CH_4$ decomposes on the Cu substrate and is converted into various carbon species such as $C_2$, $C_4$, and $C_6$ species through complex chemical reactions [92]. Figure 3.7(a) schematically depicts the simplified reaction process. $CH_4$ is dehydrogenated on the heated Cu surface and becomes $C_1$ species (C or $CH_x$). Then, two $C_1$ species combine to form $C_2$ species ($C_2$ or $C_2H_y$). The $C_2$ species can contribute to the (1) growth or (2) nucleation of graphene. The contribution to the growth seems major because $C_2$ species are considered to be stable on Cu and readily attach to the graphene edge [92]. On the other hand, $C_2$ species can further combine with other $C_2$ species to form $C_4$, $C_6$, and larger carbon species to form a graphene nucleus [92]. In short, $C_2$ species will preferentially function as the precursors for acceleration, whereas larger carbon species act as precursors for nucleation.

With the hot filament, $C_2H_2$ generated from pyrolysis is supplied on Cu and becomes $C_2$ species. Figure 3.7(b) schematically depicts the simplified reaction process of growth with the hot filament. These $C_2$ species readily attach to the graphene edge and accelerate graphene growth. At the same time, these $C_2$ species may also yield the precursors for nucleation on the heated Cu substrate. At a filament temperature of 1270 °C, the amount of these $C_2$ species is relatively low. Thus, the production of nucleation precursors is insufficient for additional nucleation, resulting in growth acceleration without nucleation. At filament temperatures > 1270 °C, a larger amount of $C_2$ species was supplied on Cu and the number of nucleation precursors exceeded the critical value for additional nucleation.

Finally, the growth rate decreased at ~1650 °C, as shown in Figure 3.6(b). This may be attributed to the decreased amount of $C_2H_2$ generated from the pyrolysis of $CH_4$. A previous report demonstrated that the formation selectivity of $C_2H_2$ in the pyrolysis of $CH_4$ by a tungsten wire decreased at ~1700 °C when the concentration of $CH_4$ was low (5 vol%) [91]. This phenomenon requires further elucidation beyond the scope of this study, which is aimed at optimizing the growth conditions for large-area single-crystalline graphene.

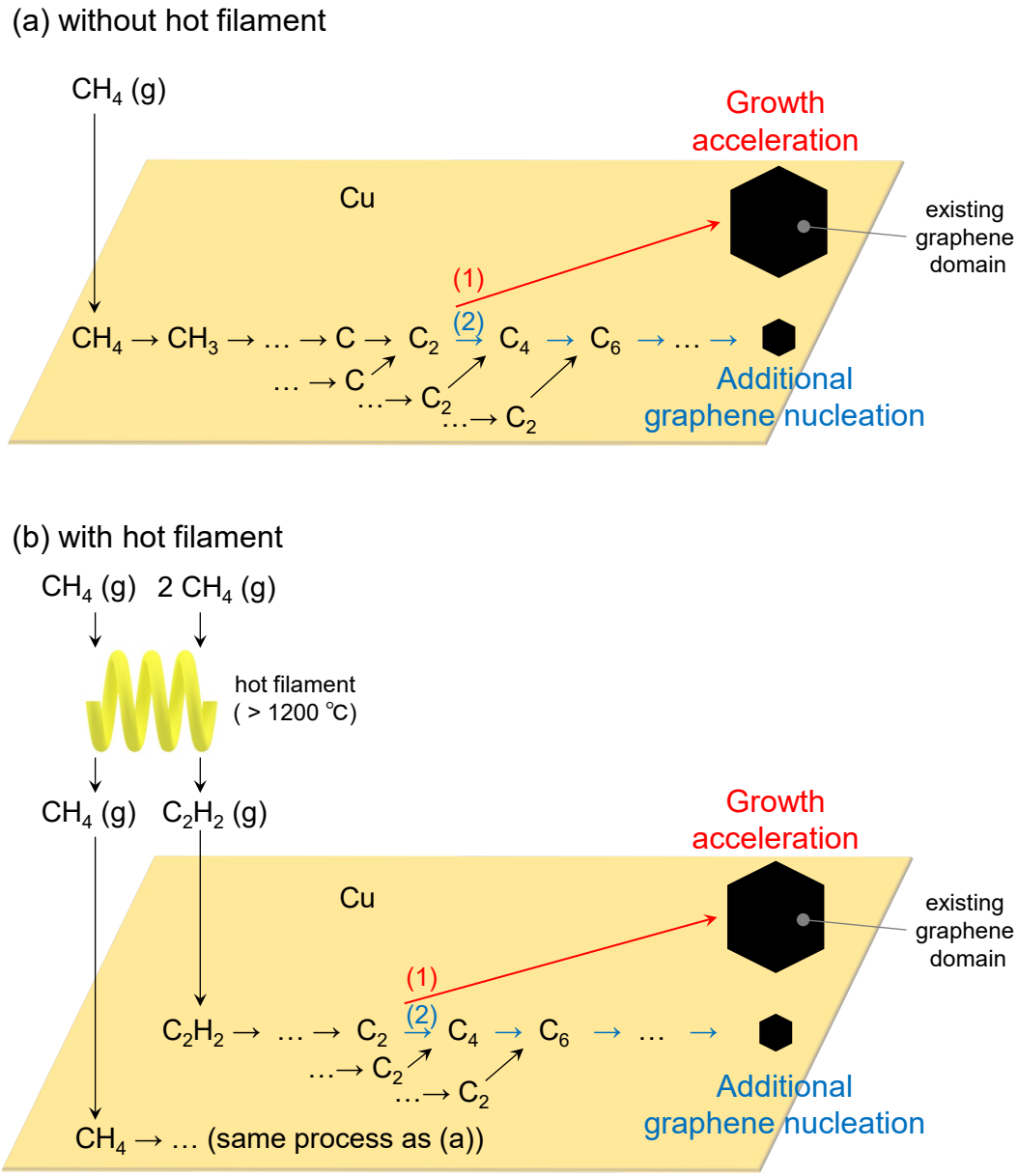


Figure 3.7 Schematic illustration of a simplified $CH_4$ decomposition process during CVD growth of graphene (a) without and (b) with the hot filament, respectively. Hydrogen atoms are not displayed. (g) indicates the gas phase. $C_2$ species contribute to (1) growth acceleration or (2) additional nucleation of graphene.

## 3.4. Conclusion

I proved that the use of the hot filament increased the precursor density on the Cu substrate in the CVD growth of graphene, resulting in the additional formation of nuclei and enhancement of growth rate. The dependence of growth rate on the filament temperature revealed an activation energy of 4.7 eV, which is close to the gas-phase dehydrogenation energy of $CH_4$. At ~1300 °C, the growth rate accelerated without additional nucleation. This phenomenon was attributed to the amount of $C_2H_2$ generated from the pyrolysis of $CH_4$ by the hot filament. At optimized temperatures, the hot filament is expected to accelerate growth without causing additional nucleation, which would be useful for rapidly synthesizing large-area single-crystalline graphene.

# Chapter 4. Effect of hydrogen

本章については、５年以内に雑誌にて刊行予定のため、非公開。

# Chapter 5. Concluding remarks

## 5.1. Conclusion

In this dissertation, I investigated the effects of the hot filament and hydrogen on the CVD growth of graphene in order to optimize these parameters for the synthesis of large-area single-crystalline graphene. For this purpose, I used Rad-OM and developed a measurement method that combined Rad-OM with SR-XPS.

The effects of the hot filament on the nucleation and growth of graphene have not been thoroughly elucidated. Using Rad-OM, I demonstrated that raising the temperature of the hot filament induced additional nucleation and enhanced the growth rate, but accelerating the growth without additional nucleation occurred at optimized filament temperatures. Thus, the hot filament would be useful for rapidly synthesizing large-area single-crystalline graphene. I proposed that the results may be attributed to the carbon species formed by the hot filament, which differ from those formed on the Cu foil substrate. The conclusion was obtained by evaluation of the nucleation and growth rate of the CVD growth of graphene using Rad-OM analysis.

The effects of hydrogen on the nucleation, growth, and etching of graphene were reported, but some effects appeared inconsistent and the critical effect has been unclear. By using Rad-OM and the combination of Rad-OM and SR-XPS, I concluded that the crucial effect of hydrogen on the CVD growth of graphene is the etching of graphene. Rad-OM revealed that the shrinkage rate during the annealing with $H_2$ was higher than that without $H_2$ and that hydrogen etched graphene. The etching effect on the growth of graphene was also demonstrated by the observation that the number of graphene domains rapidly increased after stopping the supply of $H_2$ during the growth with $H_2$. The SR-XPS measurement also confirmed the etching effect of $H_2$ based on the findings that the amount of carbon species decreased after the annealing with $H_2$, and the amount after the growth with $H_2$ was lower than that without $H_2$. Further, I discussed the formation of hexagonal graphene domains during growth with $H_2$ by the etching effect of hydrogen on the balance of the amount of carbon on the substrate, the nucleation density, and the

growth rate, obtained from the combined measurement of Rad-OM and in-situ SR-XPS. Based on the results, introducing $H_2$ is favorable for the growth of large-area and hexagonal graphene domains.

These conclusions based on in-situ Rad-OM and SR-XPS analyses will be beneficial in establishing guidelines to optimize the CVD growth of graphene and will pave the way for the production of large-area single-crystalline graphene.

## 5.2. Perspective

There are several challenges in the field of CVD growth of graphene; however, Rad-OM has the potential to address many of them. Control of the number of graphene layers has garnered tremendous research interest, but the mechanism of formation of multilayer graphene remains unclear. Rad-OM can differentiate between monolayer and multilayer graphene, and therefore has the potential to aid in elucidating the mechanism of multilayer formation.

Optimizing the CVD growth of the atomic layer materials other than graphene, such as h-BN and $MoS_2$, is important to enhance and expand their applications; however, their mechanisms of nucleation and growth have not been ascertained. Rad-OM could enable observation of the growth of these materials, provided that the emissivities of the products and the substrates are different. Rad-OM could potentially allow observation of the CVD growth of these materials and thereby provide useful information for growth optimization.

Further, I developed a measurement method that combines Rad-OM with SR-XPS and demonstrated that this in-situ observation technique could effectively analyze CVD growth. The combination of Rad-OM with other in-situ spectroscopic techniques could produce a powerful technique. For example, the combination of Rad-OM and in-situ Raman spectroscopy could potentially facilitate evaluation of the relationship between the quality of grown graphene and the nucleation density or growth rate obtained from Rad-OM without the influence of oxidation by the air or impurities in the air.

# References


[1] K. S. Novoselov *et al.*, “Electric Field Effect in Atomically Thin Carbon Films,” *Science*, vol. 306, pp. 666–669, 2004, doi: 10.1126/science.1102896.

[2] J. Chen, C. Jang, S. Xiao, M. Ishigami, and M. S. Fuhrer, “Intrinsic and extrinsic performance limits of graphene devices on $SiO_2$,” *Nat. Nanotechnol.*, vol. 3, no. 4, pp. 206–209, 2008, doi: 10.1038/nnano.2008.58.

[3] C. Lee, X. Wei, J. W. Kysar, and J. Hone, “Measurement of the Elastic Properties and Intrinsic Strength of Monolayer Graphene,” *Science*, vol. 321, no. 5887, pp. 385–388, Jul. 2008, doi: 10.1126/science.1157996.

[4] K. F. Mak, M. Y. Sfeir, Y. Wu, C. H. Lui, J. A. Misewich, and T. F. Heinz, “Measurement of the opptical conductivity of graphene,” *Phys. Rev. Lett.*, vol. 101, no. 19, pp. 2–5, 2008, doi: 10.1103/PhysRevLett.101.196405.

[5] Y. Shi *et al.*, “Synthesis of few-layer hexagonal boron nitride thin film by chemical vapor deposition,” *Nano Lett.*, vol. 10, no. 10, pp. 4134–4139, 2010, doi: 10.1021/nl1023707.

[6] Y. H. Lee *et al.*, “Synthesis of large-area $MoS_2$ atomic layers with chemical vapor deposition,” *Adv. Mater.*, vol. 24, no. 17, pp. 2320–2325, 2012, doi: 10.1002/adma.201104798.

[7] P. Vogt *et al.*, “Silicene: Compelling Experimental Evidence for Graphenelike Two-Dimensional Silicon,” *Phys. Rev. Lett.*, vol. 108, no. 15, p. 155501, Apr. 2012, doi: 10.1103/PhysRevLett.108.155501.

[8] M. E. Dávila, L. Xian, S. Cahangirov, A. Rubio, and G. Le Lay, “Germanene: a novel two-dimensional germanium allotrope akin to graphene and silicene,” *New J. Phys.*, vol. 16, no. 9, p. 095002, Sep. 2014, doi: 10.1088/1367-2630/16/9/095002.

[9] P. Solís-Fernández, M. Bissett, and H. Ago, “Synthesis, structure and applications of graphene-based 2D heterostructures,” *Chem. Soc. Rev.*, vol. 46, no. 15, pp. 4572–4613, 2017, doi: 10.1039/C7CS00160F.

[10] Q. Li, M. Liu, Y. Zhang, and Z. Liu, “Hexagonal Boron Nitride-Graphene Heterostructures: Synthesis and Interfacial Properties,” *Small*, vol. 12, no. 1, pp. 32–50, 2016, doi: 10.1002/smll.201501766.

[11] L. Banszerus *et al.*, “Ultrahigh-mobility graphene devices from chemical vapor deposition on reusable copper,” *Sci. Adv.*, vol. 1, no. 6, pp. e1500222–e1500222, 2015, doi: 10.1126/sciadv.1500222.

[12] G. Lu, L. E. Ocola, and J. Chen, “Reduced graphene oxide for room-temperature gas sensors,” *Nanotechnology*, vol. 20, no. 44, p. 445502, Nov. 2009, doi: 10.1088/0957-4484/20/44/445502.

[13] G. Seo *et al.*, “Rapid Detection of COVID-19 Causative Virus (SARS-CoV-2) in Human Nasopharyngeal Swab Specimens Using Field-Effect Transistor-Based Biosensor,” *ACS Nano*, vol. 14, no. 4, pp. 5135–5142, Apr. 2020, doi: 10.1021/acsnano.0c02823.

[14] J. Ryu *et al.*, “Fast Synthesis of High-Performance Graphene Films by Hydrogen-Free Rapid Thermal Chemical Vapor Deposition,” *ACS Nano*, vol. 8, no. 1, pp. 950–956, Jan. 2014, doi: 10.1021/nn405754d.

[15] A. Zurutuza and C. Marinelli, “Challenges and opportunities in graphene commercialization,” *Nat. Nanotechnol.*, vol. 9, no. 10, pp. 730–734, Oct. 2014, doi: 10.1038/nnano.2014.225.

[16] S. Naghdi, K. Y. Rhee, and S. J. Park, “A catalytic, catalyst-free, and roll-to-roll production of graphene via chemical vapor deposition: Low temperature growth,” *Carbon*, vol. 127, pp. 1–12, Feb. 2018, doi: 10.1016/j.carbon.2017.10.065.

[17] B. Deng, Z. Liu, and H. Peng, “Toward Mass Production of CVD Graphene Films,” *Adv. Mater.*, vol. 31, no. 9, pp. 1–25, 2019, doi: 10.1002/adma.201800996.

[18] P. Y. Huang *et al.*, “Grains and grain boundaries in single-layer graphene atomic patchwork quilts,” *Nature*, vol. 469, no. 7330, pp. 389–392, 2011, doi: 10.1038/nature09718.

[19] K. Kim *et al.*, “Ripping graphene: Preferred directions,” *Nano Lett.*, vol. 12, no. 1, pp. 293–297, 2012, doi: 10.1021/nl203547z.

[20] K. Nagashio, T. Nishimura, K. Kita, and A. Toriumi, “Mobility Variations in Mono- and Multi-Layer Graphene Films,” *Appl. Phys. Express*, vol. 2, p. 025003, Jan. 2009, doi: 10.1143/APEX.2.025003.

[21] Y. Hernandez *et al.*, “High-yield production of graphene by liquid-phase exfoliation of graphite,” *Nat. Nanotechnol.*, vol. 3, no. 9, pp. 563–568, Sep. 2008, doi: 10.1038/nnano.2008.215.

[22] K. V. Emtsev *et al.*, “Towards wafer-size graphene layers by atmospheric pressure graphitization of silicon carbide,” *Nat. Mater.*, vol. 8, no. 3, pp. 203–207, Mar. 2009, doi: 10.1038/nmat2382.

[23] X. Li *et al.*, “Large-area synthesis of high-quality and uniform graphene films on copper foils.,” *Science*, vol. 324, no. 5932, pp. 1312–1314, 2009, doi: 10.1126/science.1171245.

[24] S. Hofmann, P. Braeuninger-Weimer, and R. S. Weatherup, “CVD-Enabled Graphene Manufacture and Technology,” *J. Phys. Chem. Lett.*, vol. 6, no. 14, pp. 2714–2721, Jul. 2015, doi: 10.1021/acs.jpclett.5b01052.

[25] X. Li, L. Colombo, and R. S. Ruoff, “Synthesis of Graphene Films on Copper Foils by Chemical Vapor Deposition,” *Adv. Mater.*, pp. 6247–6252, 2016, doi: 10.1002/adma.201504760.

[26] X. Li, W. Cai, L. Colombo, and R. S. Ruoff, “Evolution of graphene growth on Ni and Cu by carbon isotope labeling,” *Nano Lett.*, vol. 9, no. 12, pp. 4268–4272, 2009, doi: 10.1021/nl902515k.

[27] M. Chen, R. C. Haddon, R. Yan, and E. Bekyarova, “Advances in transferring chemical vapour deposition graphene: a review,” *Mater. Horizons*, vol. 4, no. 6, pp. 1054–1063, 2017, doi: 10.1039/C7MH00485K.

[28] H. C. Lee, W. Liu, S. Chai, and R. Mohamed, “Review of the synthesis, transfer, characterization and growth mechanisms of single and multilayer graphene,” *RSC Adv.*, vol. 7, no. 26, p. 15644, 2017, doi: 10.1039/C7RA00392G.

[29] H. Kim *et al.*, “Copper-vapor-assisted chemical vapor deposition for high-quality and metal-free single-layer graphene on amorphous SiO2 substrate,” *ACS Nano*, vol. 7, no. 8, pp. 6575–6582, 2013, doi: 10.1021/nn402847w.

[30] S. Chen *et al.*, “Hydrogen-free synthesis of graphene–graphitic films directly on Si substrate by plasma enhanced chemical vapor deposition,” *J. Mater. Sci. Mater. Electron.*, vol. 26, no. 3, pp. 1485–1493, 2015, doi: 10.1007/s10854-014-2565-z.

[31] X. Song *et al.*, “Seed-Assisted Growth of Single-Crystalline Patterned Graphene Domains on Hexagonal Boron Nitride by Chemical Vapor Deposition,” *Nano Lett.*, vol. 16, no. 10, pp. 6109–6116, Oct. 2016, doi: 10.1021/acs.nanolett.6b02279.

[32] J. Kraus, M. Böbel, and S. Günther, “Suppressing graphene nucleation during CVD on polycrystalline Cu by controlling the carbon content of the support foils,” *Carbon*, vol. 96, pp. 153–165, 2016, doi: 10.1016/j.carbon.2015.09.048.

[33] P. Braeuninger-Weimer, B. Brennan, A. J. Pollard, and S. Hofmann, “Understanding and Controlling Cu-Catalyzed Graphene Nucleation: The Role of Impurities, Roughness, and Oxygen Scavenging,” *Chem. Mater.*, vol. 28, pp. 8905–8915, 2016, doi: 10.1021/acs.chemmater.6b03241.

[34] T. Taira, S. Obata, and K. Saiki, “Nucleation site in CVD graphene growth investigated by radiation-mode optical microscopy,” *Appl. Phys. Express*, vol. 10, no. 5, p. 055502, May 2017, doi: 10.7567/APEX.10.055502.

[35] S. Dhingra, J. Hsu, I. Vlassiouk, and B. D’Urso, “Chemical vapor deposition of graphene on large-domain ultra-flat copper,” *Carbon*, vol. 69, pp. 188–193, Apr. 2014, doi: 10.1016/j.carbon.2013.12.014.

[36] A. Ibrahim, S. Akhtar, M. Atieh, R. Karnik, and T. Laoui, “Effects of annealing on copper substrate surface morphology and graphene growth by chemical vapor deposition,” *Carbon*, vol. 94, pp. 369–377, 2015, doi: 10.1016/j.carbon.2015.06.067.

[37] G. H. Han *et al.*, “Influence of copper morphology in forming nucleation seeds for graphene growth,” *Nano Lett.*, vol. 11, no. 10, pp. 4144–4148, 2011, doi: 10.1021/nl201980p.

[38] T. Taira, S. Obata, and K. Saiki, “Effect of grain boundaries in Cu foil on CVD growth of graphene,” *Appl. Phys. Express*, vol. 10, no. 7, p. 075503, Jul. 2017,

doi: 10.7567/APEX.10.075503.

[39] X. Li *et al.*, “Graphene films with large domain size by a two-step chemical vapor deposition process,” *Nano Lett.*, vol. 10, no. 11, pp. 4328–4334, 2010, doi: 10.1021/nl101629g.

[40] Z. Li *et al.*, “Low-temperature growth of graphene by chemical vapor deposition using solid and liquid carbon sources,” *ACS Nano*, vol. 5, no. 4, pp. 3385–3390, 2011, doi: 10.1021/nn200854p.

[41] J. K. Wassei *et al.*, “Chemical vapor deposition of graphene on copper from methane, ethane and propane: Evidence for bilayer selectivity,” *Small*, vol. 8, no. 9, pp. 1415–1422, 2012, doi: 10.1002/smll.201102276.

[42] Y. Hao *et al.*, “The Role of Surface Oxygen in the Growth of Large Single-Crystal Graphene on Copper,” *Science*, vol. 342, no. 6159, pp. 720–723, Nov. 2013, doi: 10.1126/science.1243879.

[43] L. Gan and Z. Luo, “Turning off hydrogen to realize seeded growth of subcentimeter single-crystal graphene grains on copper,” *ACS Nano*, vol. 7, no. 10, pp. 9480–9488, Oct. 2013, doi: 10.1021/nn404393b.

[44] H. Zhou *et al.*, “Chemical vapour deposition growth of large single crystals of monolayer and bilayer graphene.,” *Nat. Commun.*, vol. 4, p. 2096, 2013, doi: 10.1038/ncomms3096.

[45] P. Li, Z. Li, and J. Yang, “Dominant Kinetic Pathways of Graphene Growth in Chemical Vapor Deposition: The Role of Hydrogen,” *J. Phys. Chem. C*, vol. 121, no. 46, pp. 25949–25955, Nov. 2017, doi: 10.1021/acs.jpcc.7b09622.

[46] I. Vlassiouk *et al.*, “Role of hydrogen in chemical vapor deposition growth of large single-crystal graphene,” *ACS Nano*, vol. 5, no. 7, pp. 6069–6076, Jul. 2011, doi: 10.1021/nn201978y.

[47] X. Zhang *et al.*, “Hydrogen-induced effects on the CVD growth of high-quality graphene structures,” *Nanoscale*, vol. 5, no. 18, pp. 8363–8366, 2013, doi: 10.1039/c3nr01599h.

[48] I. A. Kostogrud, K. V Trusov, and D. V Smovzh, “Influence of Gas Mixture and Temperature on AP-CVD Synthesis of Graphene on Copper Foil,” *Adv. Mater.*

*Interfaces*, vol. 3, no. 8, p. 1500823, Apr. 2016, doi: 10.1002/admi.201500823.

[49] K. Li, C. He, M. Jiao, Y. Wang, and Z. Wu, "A first-principles study on the role of hydrogen in early stage of graphene growth during the $CH_4$ dissociation on Cu (111) and Ni (111) surfaces," *Carbon*, vol. 74, pp. 255–265, 2014, doi: 10.1016/j.carbon.2014.03.030.

[50] S. Hussain *et al.*, "Physical and electrical properties of graphene grown under different hydrogen flow in low pressure chemical vapor deposition," *Nanoscale Res. Lett.*, vol. 9, no. 1, p. 546, 2014, doi: 10.1186/1556-276X-9-546.

[51] I. Mitchell and A. J. Page, "The influence of hydrogen on transition metal - Catalysed graphene nucleation," *Carbon*, vol. 128, pp. 215–223, Mar. 2018, doi: 10.1016/j.carbon.2017.11.048.

[52] M. Borah, A. K. Pathak, D. K. Singh, P. Pal, and S. R. Dhakate, "Role of limited hydrogen and flow interval on the growth of single crystal to continuous graphene by low-pressure chemical vapor deposition," *Nanotechnology*, vol. 28, no. 7, p. 075602, Feb. 2017, doi: 10.1088/1361-6528/aa527e.

[53] Y. Zhang, Z. Li, P. Kim, L. Zhang, and C. Zhou, "Anisotropic hydrogen etching of chemical vapor deposited graphene," *ACS Nano*, vol. 6, no. 1, pp. 126–132, Jan. 2012, doi: 10.1021/nn202996r.

[54] Z. M. Gebeyehu, A. Arrighi, M. V. Costache, C. M. Sotomayor-Torres, M. J. Esplandiu, and S. O. Valenzuela, "Impact of the *in situ* rise in hydrogen partial pressure on graphene shape evolution during CVD growth of graphene," *RSC Adv.*, vol. 8, no. 15, pp. 8234–8239, 2018, doi: 10.1039/C7RA13169K.

[55] S. Choubak, M. Biron, P. L. Levesque, R. Martel, and P. Desjardins, "No graphene etching in purified hydrogen," *J. Phys. Chem. Lett.*, vol. 4, no. 7, pp. 1100–1103, Apr. 2013, doi: 10.1021/jz400400u.

[56] S. Choubak, P. L. Levesque, E. Gaufres, M. Biron, P. Desjardins, and R. Martel, "Graphene CVD: Interplay between growth and etching on morphology and stacking by hydrogen and oxidizing impurities," *J. Phys. Chem. C*, vol. 118, no. 37, pp. 21532–21540, Sep. 2014, doi: 10.1021/jp5070215.

[57] S. Naghdi, K. Y. Rhee, and S. J. Park, "A catalytic, catalyst-free, and roll-to-roll

production of graphene via chemical vapor deposition: Low temperature growth," *Carbon*, vol. 127, pp. 1–12, 2018, doi: 10.1016/j.carbon.2017.10.065.

[58] Syed Muhammad Hafiz, S. K. Chong, N. M. Huang, and S. Abdul Rahman, "Fabrication of high-quality graphene by hot-filament thermal chemical vapor deposition," *Carbon*, vol. 86, pp. 1–11, May 2015, doi: 10.1016/j.carbon.2015.01.018.

[59] N. Selvakumar, B. Vadivel, D. V. S. Rao, S. B. Krupanidhi, and H. C. Barshilia, "Controlled growth of high-quality graphene using hot-filament chemical vapor deposition," *Appl. Phys. A*, vol. 122, no. 11, p. 943, 2016, doi: 10.1007/s00339-016-0483-z.

[60] T. B. Limbu *et al.*, "A Novel Approach to the Layer-Number-Controlled and Grain-Size-Controlled Growth of High Quality Graphene for Nanoelectronics," *ACS Appl. Nano Mater.*, vol. 1, no. 4, pp. 1502–1512, Apr. 2018, doi: 10.1021/acsanm.7b00410.

[61] R. Hawaldar *et al.*, "Large-area high-throughput synthesis of monolayer graphene sheet by Hot Filament Thermal Chemical Vapor Deposition," *Sci. Rep.*, vol. 2, no. 1, p. 682, Dec. 2012, doi: 10.1038/srep00682.

[62] J. Lee *et al.*, "High-angle tilt boundary graphene domain recrystallized from mobile hot-wire-assisted chemical vapor deposition system," *Nano Lett.*, vol. 14, no. 8, pp. 4352–4359, 2014, doi: 10.1021/nl5012323.

[63] E. Lee, J. Baek, J. S. Park, J. Kim, J. M. Yuk, and S. Jeon, "Effect of nucleation density on the crystallinity of graphene grown from mobile hot-wire-assisted CVD," *2D Mater.*, vol. 6, p. 011001, Sep. 2018, doi: 10.1088/2053-1583/aae21f.

[64] X. Chen *et al.*, "Chemical vapor deposition growth of 5 mm hexagonal single-crystal graphene from ethanol," *Carbon*, vol. 94, pp. 810–815, Nov. 2015, doi: 10.1016/j.carbon.2015.07.045.

[65] X. Li *et al.*, "Large-area graphene single crystals grown by low-pressure chemical vapor deposition of methane on copper," *J. Am. Chem. Soc.*, vol. 133, no. 9, pp. 2816–2819, 2011, doi: 10.1021/ja109793s.

[66] R. Wu *et al.*, "Concurrent fast growth of sub-centimeter single-crystal graphene

with controlled nucleation density in a confined channel," *Nanoscale*, vol. 9, no. 27, pp. 9631–9640, 2017, doi: 10.1039/C7NR02741A.

[67] T. Wu *et al.*, "Fast growth of inch-sized single-crystalline graphene from a controlled single nucleus on Cu–Ni alloys," *Nat. Mater.*, vol. 15, no. 1, pp. 43–47, Nov. 2015, doi: 10.1038/nmat4477.

[68] X. Xu *et al.*, "Ultrafast growth of single-crystal graphene assisted by a continuous oxygen supply," *Nat. Nanotechnol.*, vol. 11, no. 11, pp. 930–935, Aug. 2016, doi: 10.1038/nnano.2016.132.

[69] C. Jia, J. Jiang, L. Gan, and X. Guo, "Direct Optical Characterization of Graphene Growth and Domains on Growth Substrates," *Sci. Rep.*, vol. 2, pp. 1–6, 2012, doi: 10.1038/srep00707.

[70] A. C. Ferrari and D. M. Basko, "Raman spectroscopy as a versatile tool for studying the properties of graphene," *Nat. Nanotechnol.*, vol. 8, no. 4, pp. 235–246, 2013, doi: 10.1038/nnano.2013.46.

[71] W. Guo *et al.*, "Governing Rule for Dynamic Formation of Grain Boundaries in Grown Graphene," *ACS Nano*, vol. 9, no. 6, pp. 5792–5798, Jun. 2015, doi: 10.1021/acsnano.5b01827.

[72] T. Terasawa, *Radiation Microscopy on Chemical Vapor Deposition Growth of Graphene*. Dissertation, The University of Tokyo, 2015.

[73] T. Terasawa and K. Saiki, "Radiation-mode optical microscopy on the growth of graphene," *Nat. Commun.*, vol. 6, p. 6834, 2015, doi: 10.1038/ncomms7834.

[74] T. Terasawa and K. Saiki, "Effect of vapor-phase oxygen on chemical vapor deposition growth of graphene," *Appl. Phys. Express*, vol. 8, p. 035101, 2015, doi: /10.7567/APEX.8.035101.

[75] T. Terasawa, T. Taira, S. Yasuda, S. Obata, K. Saiki, and H. Asaoka, "Effect of hydrogen on chemical vapor deposition growth of graphene on Au substrates," *Jpn. J. Appl. Phys.*, vol. 58, no. SI, p. SIIB17, Aug. 2019, doi: 10.7567/1347-4065/ab19ae.

[76] E. A. Taft and H. R. Philipp, "Optical Properties of Graphite," *Phys. Rev.*, vol. 138, no. 1A, pp. A197–A202, Apr. 1965, doi: 10.1103/PhysRev.138.A197.

[77] K. G. Ramanathan and S. H. Yen, “High-temperature emissivities of copper, aluminum, and silver,” *J. Opt. Soc. Am.*, vol. 67, no. 1, p. 32, Jan. 1977, doi: 10.1364/JOSA.67.000032.

[78] The Surface Science Society of Japan, *X-ray photoelectron spectroscopy*. Maruzen, 1998.

[79] A. Jorio, M. S. Dresselhaus, R. Saito, and G. Dresselhaus, *Raman Spectroscopy in Graphene Related Systems*. Wiley, 2011.

[80] A. Toyoshima, H. Tanaka, T. Kikuchi, K. Amemiya, and K. Mase, “Present status of a new vacuum ultraviolet and soft X-ray undulator beamline BL-13A for the study of organic thin films adsorbed on surfaces,” *J. Vac. Soc. Japan*, vol. 54, no. 11, pp. 580–584, 2011, doi: 10.3131/jvsj2.54.580.

[81] Z. Yan *et al.*, “Toward the synthesis of wafer-scale single-crystal graphene on copper foils,” *ACS Nano*, vol. 6, no. 10, pp. 9110–9117, 2012, doi: 10.1021/nn303352k.

[82] A. Mohsin *et al.*, “Synthesis of millimeter-size hexagon-shaped graphene single crystals on resolidified copper,” *ACS Nano*, vol. 7, no. 10, pp. 8924–8931, 2013, doi: 10.1021/nn4034019.

[83] S. Chen *et al.*, “Millimeter-size single-crystal graphene by suppressing evaporative loss of Cu during low pressure chemical vapor deposition,” *Adv. Mater.*, vol. 25, no. 14, pp. 2062–2065, 2013, doi: 10.1002/adma.201204000.

[84] D. Ding, P. Solís-Fernández, H. Hibino, and H. Ago, “Spatially Controlled Nucleation of Single-Crystal Graphene on Cu Assisted by Stacked Ni,” *ACS Nano*, vol. 10, pp. 11196–11204, 2016, doi: 10.1021/acsnano.6b06265.

[85] V. Miseikis *et al.*, “Rapid CVD growth of millimetre-sized single crystal graphene using a cold-wall reactor,” *2D Mater.*, vol. 2, no. 1, p. 014006, 2015, doi: 10.1088/2053-1583/2/1/014006.

[86] Q. Shi *et al.*, “3D graphene-based hybrid materials: synthesis and applications in energy storage and conversion,” *Nanoscale*, vol. 8, no. 34, pp. 15414–15447, 2016, doi: 10.1039/C6NR04770J.

[87] P. H. Q. Pham, W. Zhou, N. V. Quach, J. Li, J.-G. Zheng, and P. J. Burke,

"Controlling Nucleation Density While Simultaneously Promoting Edge Growth Using Oxygen-Assisted Fast Synthesis of Isolated Large-Domain Graphene," *Chem. Mater.*, vol. 28, pp. 6511–6519, 2016, doi: 10.1021/acs.chemmater.6b01826.

[88] H. Wang *et al.*, "Surface Monocrystallization of Copper Foil for Fast Growth of Large Single-Crystal Graphene under Free Molecular Flow," *Adv. Mater.*, vol. 28, no. 40, pp. 8968–8974, Oct. 2016, doi: 10.1002/adma.201603579.

[89] J. Chen *et al.*, "Fast growth of large single-crystalline graphene assisted by sequential double oxygen passivation," *Carbon*, vol. 116, pp. 133–138, May 2017, doi: 10.1016/j.carbon.2017.01.108.

[90] C. Guéret, M. Daroux, and F. Billaud, "Methane pyrolysis: Thermodynamics," *Chem. Eng. Sci.*, vol. 52, no. 5, pp. 815–827, 1997, doi: 10.1016/S0009-2509(96)00444-7.

[91] A. V. Porsin, A. V. Kulikov, Y. I. Amosov, V. N. Rogozhnikov, and A. S. Noskov, "Acetylene synthesis by methane pyrolysis on a tungsten wire," *Theor. Found. Chem. Eng.*, vol. 48, no. 4, pp. 397–403, 2014, doi: 10.1134/S0040579514040241.

[92] R. Muñoz and C. Gómez-Aleixandre, "Review of CVD Synthesis of Graphene," *Chem. Vap. Deposition*, vol. 19, no. 10-11–12, pp. 297–322, Dec. 2013, doi: 10.1002/cvde.201300051.

[93] H. T. Nguyen, L. K. Huynh, and T. N. Truong, "Migration and desorption of hydrogen atom and molecule on/from graphene," *Carbon*, vol. 121, pp. 248–256, 2017, doi: 10.1016/j.carbon.2017.05.069.

[94] S. J. Hong *et al.*, "Chemical manipulation of edge-contact and encapsulated graphene by dissociated hydrogen adsorption," *RSC Adv.*, vol. 7, no. 10, pp. 6013–6017, 2017, doi: 10.1039/C6RA26853F.

[95] P. Zhao *et al.*, "The role of hydrogen in oxygen-assisted chemical vapor deposition growth of millimeter-sized graphene single crystals," *Nanoscale*, vol. 8, no. 14, pp. 7646–7653, 2016, doi: 10.1039/c6nr00241b.

[96] D. Ding, P. Solís-Fernández, R. M. Yunus, H. Hibino, and H. Ago, "Behavior

and role of superficial oxygen in Cu for the growth of large single-crystalline graphene," *Appl. Surf. Sci.*, vol. 408, pp. 142–149, Jun. 2017, doi: 10.1016/j.apsusc.2017.02.250.

[97] S. Shah *et al.*, "Impact of short duration, high-flow $H_2$ annealing on graphene synthesis and surface morphology with high spatial resolution assessment of coverage," *Carbon*, vol. 125, pp. 318–326, 2017, doi: 10.1016/j.carbon.2017.09.048.

[98] X. Zhang, L. Wang, J. H. Xin, B. I. Yakobson, and F. Ding, "Role of hydrogen in graphene chemical vapor deposition growth on a copper surface.," *J. Am. Chem. Soc.*, vol. 136, no. 8, pp. 3040–3047, Feb. 2014, doi: 10.1021/ja405499x.

[99] H. Q. Ta *et al.*, "Stranski–Krastanov and Volmer–Weber CVD Growth Regimes To Control the Stacking Order in Bilayer Graphene," *Nano Lett.*, vol. 16, no. 10, pp. 6403–6410, Oct. 2016, doi: 10.1021/acs.nanolett.6b02826.

[100] L. M. Malard, M. A. Pimenta, G. Dresselhaus, and M. S. Dresselhaus, "Raman spectroscopy in graphene," *Phys. Rep.*, vol. 473, no. 5–6, pp. 51–87, 2009, doi: 10.1016/j.physrep.2009.02.003.

[101] A. Siokou, F. Ravani, S. Karakalos, O. Frank, M. Kalbac, and C. Galiotis, "Surface refinement and electronic properties of graphene layers grown on copper substrate: An XPS, UPS and EELS study," *Appl. Surf. Sci.*, vol. 257, no. 23, pp. 9785–9790, 2011, doi: 10.1016/j.apsusc.2011.06.017.

[102] W. Xie, L. T. Weng, K. M. Ng, C. K. Chan, and C. M. Chan, "Clean graphene surface through high temperature annealing," *Carbon*, vol. 94, pp. 740–748, 2015, doi: 10.1016/j.carbon.2015.07.046.

[103] J. Kim *et al.*, "Distinguishing Zigzag and Armchair Edges on Graphene Nanoribbons by X-ray Photoelectron and Raman Spectroscopies," *ACS Omega*, vol. 3, no. 12, pp. 17789–17796, 2018, doi: 10.1021/acsomega.8b02744.

[104] T. Liang, C. Luan, H. Chen, and M. Xu, "Exploring oxygen in graphene chemical vapor deposition synthesis," *Nanoscale*, vol. 9, no. 11, pp. 3719–3735, 2017, doi: 10.1039/C7NR00188F.

[105] E. Meca, J. Lowengrub, H. Kim, C. Mattevi, and V. B. Shenoy, "Epitaxial

Graphene Growth and Shape Dynamics on Copper: Phase-Field Modeling and Experiments," *Nano Lett.*, vol. 13, no. 11, pp. 5692–5697, Nov. 2013, doi: 10.1021/nl4033928.

[106] J. Dong, L. Zhang, and F. Ding, "Kinetics of Graphene and 2D Materials Growth," *Adv. Mater.*, vol. 31, no. 9, pp. 1–29, 2019, doi: 10.1002/adma.201801583.

[107] H. Shu, X. Chen, and F. Ding, "The edge termination controlled kinetics in graphene chemical vapor deposition growth," *Chem. Sci.*, vol. 5, no. 12, pp. 4639–4645, 2014, doi: 10.1039/c4sc02223h.

[108] D. H. Jung, C. Kang, D. Yoon, H. Cheong, and J. S. Lee, "Anisotropic behavior of hydrogen in the formation of pentagonal graphene domains," *Carbon*, vol. 89, pp. 242–248, Aug. 2015, doi: 10.1016/j.carbon.2015.03.034.

# Publication related to this dissertation

## Chapter 3:

[109] T. Taira, T. Shinohara, S. Obata, and K. Saiki, "Real-time observation on hot-filament-assisted CVD growth of graphene," Jpn. J. Appl. Phys., vol. 58, no. SI, p. SIIB24, Aug. 2019, doi: 10.7567/1347-4065/ab106f.

# Acknowledgment

First of all, I am sincerely grateful to Professor Jun Yoshinobu. He always kindly taught me everything about the research: fundamental knowledge, experimental technique, data analysis and interpretation, presentation, writing, and a positive attitude to the research. Without his support, I could not complete this dissertation.

I am really thankful to Dr. Shunsuke Tanaka. He helped my experiments and gave me a lot of advice for improving my experiments and thoughts. Discussion with him were powerful driving forces for my research.

I am very thankful to Mr. Kozo Mukai. He taught me how to use SES200 at KEK-PF and gave me a lot of advice and help for improving the experimental setup and their safety both at KEK-PF and Kashiwa.

I greatly appreciate the support from Mr. Younghyun Choi at KEK-PF. He cleaned my Cu foil substrate by the 10 cycles of annealing and Ar bombardment overnight. His perfect cleaning enabled me to clearly evaluate the carbon species after the CVD growth.

I deeply appreciate the help from Mr. Yu Tsuchihara. He assisted in the construction of my experimental setup and measurements at KEK-PF and allowed me to focus on my CVD experiments.

My thanks go to all the other members of Yoshinobu laboratory and Ms. Ikumi Saito and Ms. Yukiko Yagihashi for their kind help.

I heartily thank the members of Saiki laboratory.

Professor Koichiro Saiki encouraged me to succeed to Dr. Terasawa's research when I was an undergraduate student. During my doctorial course, he instructed the research of HF-CVD and allowed me to use the Rad-OM setup.

Dr. Seiji Obata supported the experiments and discussion of HF-CVD and helped the moving of the Rad-OM setup from Saiki laboratory to Yoshinobu laboratory.

Dr. Tomoo Terasawa, a developer of Rad-OM, kindly taught me everything about Rad-OM when I was an undergraduate student. During my doctorial course, he helped the moving of the Rad-OM setup.

Mr. Takuya Shinohara taught me how to make a W filament and helped the construction of the experimental setup for HF-CVD.

I express my deep gratitude to the people concerning the experiments at KEK-PF.

Professor Kazuhiko Mase kindly helped me to solve the experimental problem at KEK-PF BL-13B.

Dr. Kenichi Ozawa gave me chances to use SES200 at KEK-PF BL-13B as a leader of a project: 2018S2-005.

Professor Yoshinori Kitajima carefully checked the safety of my gas line.

I acknowledge the financial supports for my research and living from Japan Society for the Promotion of Science (JSPS-DC1).

Finally, I heartily thank my family for supporting my life.